Zigzag and Breakup Instabilities of Stripes and Rings in the Two-Dimensional Gray-Scott Model

T. KOLOKOLNIKOV, M. J. WARD, and J. W E I

Theodore Kolokolnikov; Dept. of Mathematics, University of British Columbia, Vancouver, Canada V6T 1Z2,
Michael Ward; Dept. of Mathematics, University of British Columbia, Vancouver, Canada V6T 1Z2 (corresponding author)
Juncheng Wei; Dept. of Mathematics, Chinese University of Hong Kong, New Territories, Hong Kong.

(*Received 24th February 2005*)

Two different types of instabilities of equilibrium stripe and ring solutions are studied for the singularly perturbed two-component Gray-Scott (GS) model in a two-dimensional domain. The analysis is performed in the semi-strong interaction limit where the ratio $O(\varepsilon^{-2})$ of the two diffusion coefficients is asymptotically large. For $\varepsilon \to 0$, an equilibrium stripe solution is constructed where the singularly perturbed component concentrates along the midline of a rectangular domain. An equilibrium ring solution occurs when this component concentrates on some circle that lies concentrically within a circular cylindrical domain. For both the stripe and the ring, the spectrum of the linearized problem is studied with respect to transverse (zigzag) and varicose (breakup) instabilities. Zigzag instabilities are associated with eigenvalues that are asymptotically small as $\varepsilon \to 0$. Breakup instabilities, associated with eigenvalues that are $O(1)$ as $\varepsilon \to 0$, are shown to lead to the disintegration of a stripe or a ring into spots. For both the stripe and the ring, a combination of asymptotic and numerical methods are used to determine precise instability bands of wavenumbers for both types of instabilities. The instability bands depend on the relative magnitude, with respect to ε, of a non-dimensional feed-rate parameter A of the GS model. Both the high feed-rate regime $A = O(1)$, where self-replication phenomena occurs, and the intermediate regime $O(\varepsilon^{1/2}) \ll A \ll O(1)$ are studied. In both regimes, it is shown that the instability bands for zigzag and breakup instabilities overlap, but that a zigzag instability is always accompanied by a breakup instability. The stability results are confirmed by full numerical simulations. Finally, in the weak interaction regime, where both components of the GS model are singularly perturbed, it is shown from a numerical computation of an eigenvalue problem that there is a parameter set where a zigzag instability can occur with no breakup instability. From full-scale numerical computations of the GS, it is shown that this instability leads to a large-scale labyrinthine pattern.

1 Introduction

Stripe or ring patterns have been observed in many numerical simulations of various classes of singularly perturbed reaction-diffusion systems. They occur for activator-inhibitor systems such as the well-known Gierer-Meinhardt model and related activator-inhibitor systems (cf. [**9**], [**16**], [**27**], [**50**], Chapter 15 of [**15**]), for certain hybrid chemotaxis reaction-diffusion models of bacterial pattern formation (cf. [**41**], [**48**], Chapter 5 of [**32**]) and of fish skin patterns on growing domains (cf. [**35**], [**36**]), and for nonlocal models of the microwave heating of ceramics [**4**], etc. In many instances a stripe or ring pattern is unstable to a varicose instability, which leads to the disintegration of the stripe or ring into a sequence of spots (cf. [**4**], [**41**], [**48**], Chapter 5 of [**32**]). In other cases, a stripe is de-stabilized by a transverse instability, which numerically seems to be the precursor to

a complicated space-filling curve (cf. [**16**], [**50**]). Most previous studies of the onset of these types of instabilities have been based on a weakly nonlinear theory near some spatially uniform steady-state (see Chapter 5 of [**32**]).

The goal of this paper is to use matched asymptotic analysis to study the onset of varicose and zigzag instabilities of equilibrium stripe and ring solutions to the singularly perturbed Gray-Scott (GS) system in a bounded two-dimensional domain Ω. Since these patterns are spatially localized and deviate substantially from a spatially uniform steady-state, a conventional Turing-type stability analysis is not applicable. The GS system models an irreversible reaction involving two reactants in a gel reactor, where the reactor is maintained in contact with a reservoir of one of the two chemical species. The dimensionless GS model is (cf. [**29**], [**17**])

$$v_t = \varepsilon_0^2 \Delta v - v + A u v^2\,, \quad X \in \Omega\,, \quad t > 0\,; \qquad \partial_n v = 0\,, \quad X \in \partial\Omega\,, \tag{1.1 a}$$

$$\tau u_t = D\Delta u - u + 1 - u v^2\,, \quad X \in \Omega\,, \quad t > 0\,; \qquad \partial_n u = 0\,, \quad X \in \partial\Omega\,. \tag{1.1 b}$$

Here $D > 0$, $\tau > 1$, $A > 0$, and $0 < \varepsilon_0 \ll 1$ are constants. The dynamics under the kinetics of (1.1), representing a continuously stirred reactor, were first introduced and studied in [**11**].

There are two key parameter regimes where (1.1) admits spatially localized solutions. In the weak interaction regime, where $D = O(\varepsilon_0^2) \ll 1$, the numerical study of [**37**] showed a plethora of patterns where both the u and v components are localized at certain points (i.e. spots) or along certain curves (i.e. stripes) in the domain. These patterns include temporally oscillating spots, spot annihilation due to over-crowding,, spot-replication behavior, spatio-temporal chaos of spot patterns, mixed spot-stripe patterns, and labyrinthine patterns of stripes. The diversity of the computed patterns are shown on the website XMORPHIA [**49**]. Many of the numerically computed patterns for the GS model have been observed qualitatively in certain chemical experiments (cf. [**23**], [**24**]). In the one-dimensional case there has been much theoretical work to classify localized pattern formation in the weak interaction regime including, the self-replication and dynamics of pulses (cf. [**8**], [**33**], [**42**]), spatio-temporal chaos and Turing structures (cf. [**26**], [**34**]), and the existence of equilibrium solutions (cf. [**14**]). In the semi-strong interaction regime $\varepsilon_0^2 \ll 1$ with $D = O(1)$, where only the v component is localized, there are many results for the existence and stability of spike patterns in one spatial dimension (cf. [**5**], [**6**], [**29**], [**30**], [**17**], [**18**], [**38**], [**39**]), and for spot patterns in two space dimensions (cf. [**31**], [**44**], [**45**], [**46**], [**47**]).

We will study the stability of equilibrium stripe and ring solutions to the GS model (1.1) in a rectangular domain and circular cylindrical domain, respectively, given by

$$\Omega:\ -1 < X_1 < 1\,, \quad 0 < X_2 < d_0 \quad \text{(rectangle)}; \qquad \Omega:\ 0 < X_1^2 + X_2^2 < 1\,, \quad \text{(disk)}\,. \tag{1.2}$$

The equilibrium stripe that we will analyze is a stripe of zero curvature that is obtained when v concentrates along the mid-line $X_1 = 0$ of the rectangular domain. Alternatively, an equilibrium ring solution occurs when v concentrates on some circle that lies concentrically within the unit disk. For the analysis, it is convenient to introduce a new spatial variable $x = (x_1, x_2)$ by $x = lX$, where $l \equiv D^{-1/2}$. In terms of x, (1.1) becomes

$$v_t = \varepsilon^2 \Delta v - v + A u v^2\,, \quad x \in \Omega\,, \quad t > 0\,; \qquad \partial_n v = 0\,, \quad x \in \partial\Omega\,, \tag{1.3 a}$$

$$\tau u_t = \Delta u - u + 1 - u v^2\,, \quad x \in \Omega\,, \quad t > 0\,; \qquad \partial_n u = 0\,, \quad x \in \partial\Omega\,. \tag{1.3 b}$$

In (1.3), ε and the new domain Ω are defined by

$$\Omega:\ -l < x_1 < l\,,\quad 0 < x_2 < d \equiv l d_0 \quad \text{(rectangle)}; \qquad \Omega:\ 0 < x_1^2 + x_2^2 < R^2 \equiv l^2\,,\quad \text{(disk)}\,, \tag{1.3 c}$$

$$\varepsilon \equiv \varepsilon_0 l = \varepsilon_0/\sqrt{D}\,. \tag{1.3 d}$$

The semi-strong interaction regime is $\varepsilon \ll 1$, while the weak interaction regime is $l \gg 1$ with $\varepsilon = O(1)$.

In the semi-strong interaction regime, we analyze the stability of rings and stripes with respect to zigzag (transverse) and breakup (varicose) instabilities. The zigzag instability, such as shown in Fig. 10 below, is associated with the eigenvalues of the linearization that tend to zero as $\varepsilon \to 0$, referred to as the small eigenvalues. The corresponding eigenfunctions for both u and v are, locally, odd functions near the stripe or the ring. The breakup instability is associated with the large eigenvalues of the linearization that are $O(1)$ as $\varepsilon \to 0$. The corresponding eigenfunctions for both u and v are, locally, even functions near the stripe or the ring. This type of instability is found to lead to the disintegration of the ring or stripe into spots, such as shown below in Fig. 12.

In the semi-strong interaction regime, equilibrium ring solutions were constructed in [**28**] and [**22**] for the GS model (1.3) in the low feed-rate regime $A = O(\varepsilon^{1/2})$, and their stability properties were analyzed with respect to breakup instabilities. It was shown in [**22**] that a ring solution in this regime is unstable with respect to spatial perturbations in v of the form $\cos(m\theta)\phi$, where ϕ is an even function near the ring, for modes m that satisfy $m_1 \le m \le m_2$. Here $m_1 = O(1)$ and $m_2 = O(\varepsilon^{-1})$ as $\varepsilon \to 0$. Furthermore, it was shown in [**22**] that m_1 increases as A is increased. A natural question then is whether the instability band disappears for some A on the range $A \gg O(\varepsilon^{1/2})$, leading to a ring that is stable with respect to breakup instabilities.

In the semi-strong interaction regime, we use a combination of formal asymptotic and numerical methods to investigate this specific question and, more generally, to give precise results for the existence of zigzag and breakup instabilities of equilibrium stripe and ring solutions when $A \gg O(\varepsilon^{1/2})$. There are two key regimes

$$\text{Intermediate regime:}\quad O(\varepsilon^{1/2}) \ll A \ll O(1)\,; \qquad \text{High feed-rate regime:}\quad A = O(1)\,.$$

Self-replication behavior of a ring, leading to a multiple ring solution, is known to occur in the high feed-rate regime (see §9 of [**22**] and §5 of [**28**]). Since pulse-splitting also occurs in this regime in the one-dimensional case (cf. [**5**], [**29**], [**17**]), this suggests the phenomena of stripe replication in a rectangular domain when $A = O(1)$.

For breakup instabilities of stripes and rings, we show that the unstable modes m in the high feed-rate regime satisfy $m_l < \varepsilon m < m_u$ for some $O(1)$ thresholds m_l and m_u. Thus, the unstable modes are of the order $m = O(\varepsilon^{-1})$. In the intermediate regime m_u and m_l are calculated analytically, and it is shown that $m_l = O(A^2)$ for $O(\varepsilon^{1/2}) \ll A \ll O(1)$. The results for breakup instabilities of stripes and rings are given in Principal Results 4.2 and 5.5, respectively. Therefore, breakup instabilities always occur in the regime $A \gg O(\varepsilon^{1/2})$.

For zigzag instabilities, we also show that there exists a band of unstable modes, for both the stripe and the ring, in the high feed-rate and intermediate regimes. More specifically, in the high feed-rate regime, we show that all unstable zigzag modes m satisfy $m_b \le m \le \varepsilon^{-1} m_u$ for some thresholds m_b and m_u. The key results for zigzag instabilities of stripes and rings are given in Principal Result 3.2 and Principal Result 5.4, respectively. For a stripe solution in the intermediate regime, we calculate $m_u \sim O(A^2)$ for $O(\varepsilon^{1/2}) \ll A \ll O(1)$.

Our instability results in the semi-strong regime are interpreted qualitatively and compared with full numerical computations of the GS model (1.3). For a stripe solution, the upper bound of the instability band sets a critical domain size for the existence of zigzag or breakup instabilities. Since the upper bound is $O(\varepsilon^{-1})$ in the high feed-rate regime, it follows that a stripe in this regime can be stable with respect to zigzag and breakup instabilities only when the domain width d_0 in (1.3 c) is $O(\varepsilon)$ thin. In addition, in both the intermediate and high-feed rate regimes, the instability bands for zigzag and breakup instabilities are shown to overlap in such a way that a zigzag instability is always accompanied by a breakup instability. Since the width of the instability band is $O(\varepsilon^{-1})$, this suggests the possibility that either the zigzag or breakup instability band can disappear in the weak interaction regime where $l \to \infty$ and $\varepsilon = O(1)$. In this regime, where both u and v are localized, a numerical study of an eigenvalue problem shows that there is a parameter set where a zigzag instability can occur with no breakup instability. This type of instability is shown to be precursor to a large-scale labyrinthine pattern.

For the related generalized Gierer-Meinhardt (GM) model (cf. [**9**], [**27**]), the stability of a stripe solution on the infinite strip $\mathbb{R}^1 \times (0, d)$ was analyzed in [**7**] with respect to breakup instabilities. In the semi-strong interaction regime it was shown analytically that a stripe is stable to breakup instabilities only for thin domains. In the weak interaction regime, self-replicating stripes were studied in [**7**] and it was shown from full numerical simulations of the classical GM model that a stripe can become stable with respect to breakup instabilities. We qualitatively compare our results for the GS model (1.3) with these previous results of [**7**] for stripes in the GM model, and we discuss some new results of [**19**] for the finite rectangular domain $(-1, 1) \times (0, d)$. These results for the GM model are shown to be qualitatively very similar to those for the GS model (1.3) in the low feed-rate regime.

For bistable systems, such as the Fitzhugh-Nagumo model, there have been several stability analyses relating to a different class of stripe-type solutions. In [**12**] a phase equation was used to analyze zigzag instabilities of periodic stripe solutions of the Fitzhugh-Nagumo model. For this model, labyrinthine patterns of stripes were studied both analytically and numerically in [**10**] from a contour dynamics approach. In [**13**] zigzag and breakup instabilities of a stripe in an unbounded domain were studied for a reaction-diffusion system with piecewise linear kinetics. For bistable systems, where the cross-section of the stripe is composed of two transition layers joined together by an, essentially, flat plateau, the spectrum of the linearization contains only the small eigenvalues that tend to zero with the thickness ε of the interface. Therefore, for such systems, there are no breakup instabilities and the unstable small eigenvalues lead to zigzag instabilities. A rigorous stability analysis of this type of stripe solution to zigzag perturbations was given in [**40**] for a general class of bistable reaction-diffusion systems.

The outline is as follows. In §2 we construct an equilibrium stripe solution in the intermediate and high feed-rate regimes. In §3 and §4 we analyze the stability of a stripe with respect to zigzag and breakup instabilities, respectively. Analogous results for a ring are given in §5. In §6 we discuss our results qualitatively, and in relation to similar results for the GM model. We also give some numerical results for instability bands in the weak interaction regime. Full numerical results are given in §7. A brief conclusion is given in §8. In Appendix B we compare our results for breakup instabilities of a ring in the intermediate regime with those of [**28**].

2 Asymptotic Construction of a Stripe Equilibrium

For $\varepsilon \to 0$, we construct a stripe equilibrium solution to (1.3) in the rectangular domain $\Omega = [-l, l] \times [0, d]$. Since stripes are inherently one-dimensional, the analysis is the same as in §2 of [**17**] for the one-dimensional GS model. We now outline that part of this previous work which is needed in the stability analysis of §3 and §4.

In the high feed-rate regime, where $A = O(1)$, we seek an inner solution in the spike core in the form $v = \varepsilon^{-1} V$, $u = \varepsilon U/A$, and $y = \varepsilon^{-1} x_1$ (see §2 of [**17**]). Here V and U are $O(1)$, and $x_1 \in [-l, l]$ is the first component of $x = (x_1, x_2)$. Introducing these variables into the steady-state problem for (1.3), we obtain

$$V'' - V + V^2 U = 0\,, \qquad U'' - \varepsilon^2 U + A\varepsilon - V^2 U = 0\,. \tag{2.1}$$

Therefore, since $A = O(1)$, we expand V and U as

$$V = V_0(y) + A\varepsilon V_1(y) + \cdots\,, \qquad U = U_0(y) + A\varepsilon U_1(y) + \cdots\,. \tag{2.2}$$

Substituting (2.2) into (2.1), and collecting powers of εA, we obtain on $-\infty < y < \infty$ that

$$V_0'' - V_0 + V_0^2 U_0 = 0\,, \qquad U_0'' - V_0^2 U_0 = 0\,, \tag{2.3 a}$$

$$V_1'' - V_1 + 2V_0 U_0 V_1 + V_0^2 U_1 = 0\,, \qquad U_1'' + 1 - 2V_0 U_0 V_1 - V_0^2 U_1 = 0\,. \tag{2.3 b}$$

The far-field conditions for V_j are that $V_j \to 0$ as $|y| \to \infty$ for $j = 0, 1$. The far-field conditions for U_j are found below by matching U_j to the outer solution.

Next, we consider the outer region. Since v is exponentially small in this region, we need only analyze u. We first use the inner solution to calculate uv^2 in the sense of distributions. This yields

$$uv^2 \to C_0 \delta(x_1) + \varepsilon C_1 \delta(x_1) + \cdots\,, \qquad C_0 = \frac{1}{A}\int_{-\infty}^{\infty} U_0 V_0^2\, dy\,, \qquad C_1 = \int_{-\infty}^{\infty} \left(2U_0 V_0 V_1 + V_0^2 U_1\right)\, dy\,. \tag{2.4}$$

Substituting (2.4) into (1.3), we obtain the outer problem for u

$$u_{x_1 x_1} + (1 - u) = C_0 \delta(x_1) + \varepsilon C_1 \delta(x_1) + \cdots\,, \quad -l < x_1 < l\,; \qquad u_{x_1}(\pm l) = 0\,. \tag{2.5}$$

Therefore, a two-term expansion for the outer solution is

$$u = 1 - C_0 G_l(x_1) - \varepsilon C_1 G_l(x_1) + \cdots\,. \tag{2.6}$$

Here $G_l(x_1)$ is the Green's function on $-l < x_1 < l$, which is given as the solution to

$$G_{l x_1 x_1} - G_l = -\delta(x_1)\,, \quad -l < x_1 < l\,; \qquad G_{l x_1}(\pm l) = 0\,; \qquad G_l(x_1) = \frac{\cosh\left(l - |x_1|\right)}{2\sinh\left(l\right)}\,. \tag{2.7}$$

To match the inner and outer expansions for u we require that

$$\frac{\varepsilon}{A}\left(U_0(y) + A\varepsilon U_1(y) + \cdots\right) \sim 1 - C_0 G_l(\varepsilon y) - \varepsilon C_1 G_l(\varepsilon y) + \cdots\,. \tag{2.8}$$

This matching condition yields that $1 - C_0 G_l(0) = 0$, and $U_0(y) \sim -A C_0 G_{l x_1}(0^{\pm}) y$ as $y \to \pm\infty$. By calculating $G_l(0)$, $G_{l x_1}(0^{\pm})$ from (2.7), we obtain that $C_0 = 2\tanh(l)$, and

$$U_0 \sim B|y|\,, \quad \text{as} \quad |y| \to \infty\,, \qquad B \equiv \frac{C_0 A}{2} = A\tanh(l)\,. \tag{2.9}$$

In terms of the solution to (2.3 a) with the far-field condition (2.9), there is a constant $E = E(B)$ such that

$$U_0 - B|y| \to E\,, \qquad \text{as} \quad |y| \to \infty\,. \tag{2.10}$$

Substituting this expression into the matching condition (2.8), and calculating $G_l(0)$, $G_{lx_1}(0^{\pm})$, and $G_{lx_1x_1}(0)$, we obtain that $C_1 = -2EA^{-1}\tanh(l)$, together with the asymptotic boundary condition

$$U_1 \sim -\frac{y^2}{2} - \frac{E}{B}\left(\tanh^2 l\right)|y|\,, \quad \text{as} \quad |y| \to \infty\,. \tag{2.11}$$

The problem for U_1, V_1 is then (2.3 b) together with $V_1 \to 0$ as $|y| \to \infty$ and (2.11) for U_1.

We label the *core problem* as (2.3 a), together with $U_0'(0) = V_0'(0) = 0$, and the far-field boundary conditions (2.9) and $V_0(\pm\infty) = 0$. In [**29**] and [**17**] it was shown numerically that a one-bump solution to this core problem exists only for $B < 1.347$. The existence of this fold point was proved in [**5**] using a topological shooting method. To compute solution branches to the core problem, it is convenient to define γ by (cf. [**17**])

$$\gamma \equiv V_0(0)U_0(0)\,. \tag{2.12}$$

In [**17**] it was shown that $0 \le \gamma \le \frac{3}{2}$. For each value of γ on this range a value of B can be computed numerically. The resulting plot is shown in Fig. 1, which has a fold point at $\gamma = 1.02$ and $B = 1.347$. We refer to the range $1.02 < \gamma < 1.5$ and $0 < \gamma < 1.02$ as the *primary* and *secondary* solution branches, respectively. We summarize the asymptotic construction of a one-stripe equilibrium solution for (1.3) as follows:

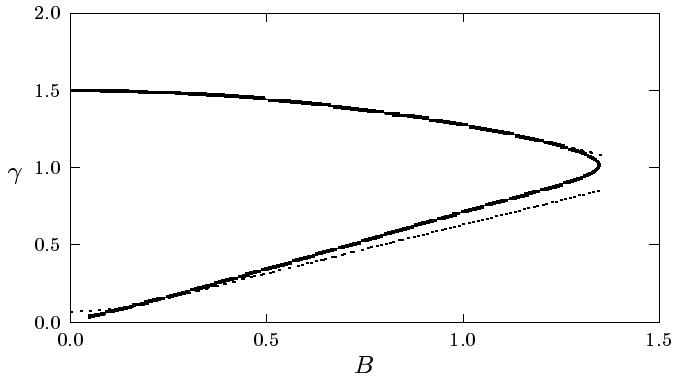

FIGURE 1. Plot of $\gamma = V_0(0)U_0(0)$ versus $B = U_0'(\infty)$, with fold point at $\gamma = 1.02$, $B = 1.347$. The dotted curves represent asymptotic approximations to the curve as derived in §3 of [**17**]. The top branch is the primary branch.

Principal Result 2.1: *Let $\Omega = [-l, l] \times [0, d]$, and define B by*

$$B = A\tanh l\,. \tag{2.13}$$

Suppose that $A = O(1)$ and $B < 1.347$. Then, along the primary branch of the γ versus B curve, there exists an equilibrium stripe solution to (1.3) of the form

$$v_e \sim \frac{1}{\varepsilon}\left(V_0(y) + \varepsilon V_1(y) + \cdots\right)\,, \qquad u_e \sim \frac{\varepsilon}{A}\left(U_0(y) + \varepsilon U_1(y) + \cdots\right)\,, \qquad y = \varepsilon^{-1}x_1\,, \tag{2.14}$$

where $V_0(y)$, $U_0(y)$ are even solutions to (2.3 a) subject to the boundary conditions

$$V_0^{'}(0) = U_0^{'}(0) = 0\,, \qquad V_0(\infty) = 0\,, \qquad U_0^{\prime}(\infty) = B\,. \tag{2.15}$$

In the outer region, v_e is exponentially small, and the leading-order approximation to u_e is

$$u_e \sim 1 - \tanh l \left(\frac{\cosh(l - |x_1|)}{\sinh(l)} \right) + O(\varepsilon)\,. \tag{2.16}$$

For the one-dimensional GS model on $|x| \le l$ pulse-splitting occurs for values of A that exceed the fold-point value $A = 1.347 \coth l$ (cf. [**5**], [**17**]). For the infinite-line problem where $l = \infty$, the core problem was introduced in [**29**] and was also given in a different form as the leading terms in equation (2.9) of [**6**]. For the finite-domain problem, the numerical evidence in Table 3 of [**5**] suggested the fold point value $A = 1.347 \coth l$. However, the derivation of this result, based on inner-matching matching, was first given in [**17**]. In general, the core problem (2.3 *a*) and (2.15) must be solved numerically. However, for $B \ll 1$, one can obtain an asymptotic solution of this problem for the two extreme limits of the $\gamma = \gamma(B)$ curve. At the edge of the primary solution branch where $\gamma \to 3/2$ from below, the following result, given in Principal Result 3.1 of [**17**], shows the merging of the high feed-rate solution where $A = O(1)$ to the intermediate regime solution where $O(\varepsilon^{1/2}) \ll A \ll O(1)$:

Principal Result 2.2: *In the intermediate regime we have*

$$B = A \tanh l \sim 3\delta \quad \text{with} \quad O(\varepsilon^{1/2}) \ll \delta \ll O(1)\,. \tag{2.17}$$

In this limit, the core problem (2.3 a) with boundary conditions (2.15) admits the limiting stripe solution

$$V_0(y) \sim \delta \left(w(y) + \delta^2 v_1(y) + \cdots \right)\,, \qquad U_0(y) \sim \delta^{-1} \left(1 + \delta^2 u_1(y) + \cdots \right)\,, \tag{2.18}$$

where $w(y) = \frac{3}{2} sech^2\,(y/2)$ is the unique solution to

$$w'' - w + w^2 = 0 \qquad w'(0) = 0\,, \quad w(0) > 0\,, \quad w \to 0 \ \text{ as } \ |y| \to \infty\,. \tag{2.19}$$

The correction terms u_1 and v_1 satisfy

$$u_1'' = w^2\,, \quad u_1'(0) = u_1(0) = 0\,; \qquad v_1'' - v_1 + 2wv_1 = -w^2 u_1\,, \quad v_1'(0) = 0\,, \quad v_1 \to 0 \ \text{ as } \ |y| \to \infty\,. \tag{2.20}$$

The corresponding local behavior of the γ versus B curve is $\gamma \equiv U_0(0)V_0(0) \sim \frac{3}{2} - \frac{11B^2}{48}$.

A similar asymptotic construction can be done to calculate the local behavior of the γ versus B curve valid for $\gamma \to 0^+$. This latter result shows that $\gamma \sim \sqrt{2}B/\sqrt{5}$ (see Principal Result 3.2 of [**17**]). In Fig. 1 the dotted lines correspond to the two local behaviors of the γ versus B curve for $\gamma \to 0^+$ and $\gamma \to (3/2)^-$.

3 Zigzag Instabilities of a Stripe

We now study zigzag instabilities of the equilibrium stripe solution u_e, v_e of (1.3) constructed in §2 along the primary solution branch of the $\gamma = \gamma(B)$ curve. We introduce the perturbation

$$v = v_e + e^{\lambda t} e^{imx_2} \phi\,, \qquad u = u_e + e^{\lambda t} e^{imx_2} \eta\,, \qquad m = \frac{k\pi}{d}\,, \quad k = 1, 2, \ldots\,, \tag{3.1}$$

where $\phi = \phi(x_1) \ll 1$ and $\eta = \eta(x_1) \ll 1$. The relationship above between m and k follows from the Neumann conditions on $x_2 = 0, d$ of $\partial\Omega$. In the analysis below, we treat m as a continuous variable. The band of instability with respect to m that is determined below can be mapped to a k-band of instability using (3.1).

Substituting (3.1) into (1.3), we obtain the following eigenvalue problem on $-l < x_1 < l$:

$$\lambda\phi = \varepsilon^2\phi_{x_1x_1} - \varepsilon^2 m^2\phi - \phi + 2Au_ev_e\phi + Av_e^2\eta\,, \qquad \tau\lambda\eta = \eta_{x_1x_1} - m^2\eta - \eta - 2u_ev_e\phi - v_e^2\eta\,. \tag{3.2}$$

This problem is studied in the inner region, where $y = \varepsilon^{-1}x_1 = O(1)$, and in the outer region, where $|x_1| \gg O(\varepsilon)$.

In the inner region, the equilibrium solution is given by (2.14). Therefore, in this region we write

$$u_e = \frac{\varepsilon}{A}U\,, \quad v_e = \frac{V}{\varepsilon}\,, \quad \phi = \frac{1}{\varepsilon}\Phi\,, \quad \eta = \frac{\varepsilon}{A}N\,, \quad y = \varepsilon^{-1}x_1\,. \tag{3.3}$$

With these inner variables, (3.2) is transformed to the following eigenvalue problem on $-\infty < y < \infty$:

$$\lambda\Phi = \Phi'' - (1 + m^2\varepsilon^2)\Phi + V^2N + 2VU\Phi\,, \qquad \tau\varepsilon^2\lambda N = N'' - \varepsilon^2\left(m^2+1\right)N - V^2N - 2VU\Phi\,. \tag{3.4}$$

From (2.2), V and U can be expanded in powers of εA. Therefore, a dominant balance argument suggests that

$$\Phi = \Phi_0 + \varepsilon A\Phi_1 + \cdots\,, \qquad N = N_0 + \varepsilon AN_1 + \cdots\,, \qquad \lambda = \varepsilon A\lambda_0 + \cdots\,. \tag{3.5}$$

We first assume that $m = O(1)$ as $\varepsilon \to 0$. Substituting (2.2) and (3.5) into (3.4), and collecting powers of εA, we obtain the following problems on $-\infty < y < \infty$:

$$L\begin{pmatrix}\Phi_0\\ N_0\end{pmatrix} \equiv \begin{pmatrix}\Phi_0''\\ N_0''\end{pmatrix} + \mathcal{E}\begin{pmatrix}\Phi_0\\ N_0\end{pmatrix} = 0\,, \qquad \mathcal{E} \equiv \begin{pmatrix}-1+2V_0U_0 & V_0^2\\ -2V_0U_0 & -V_0^2\end{pmatrix}\,, \tag{3.6}$$

and

$$L\Psi = \begin{pmatrix}\lambda_0 & 0\\ 0 & 0\end{pmatrix}\begin{pmatrix}\Phi_0\\ N_0\end{pmatrix} + \begin{pmatrix}-2(V_0U_1+U_0V_1) & -2V_0V_1\\ 2(V_0U_1+U_0V_1) & 2V_0V_1\end{pmatrix}\begin{pmatrix}\Phi_0\\ N_0\end{pmatrix}\,, \qquad \Psi \equiv \begin{pmatrix}\Phi_1\\ N_1\end{pmatrix}\,. \tag{3.7}$$

The odd solution to the leading-order system (3.6) is

$$\Phi_0 = V_0'\,, \qquad N_0 = U_0'\,. \tag{3.8}$$

To determine λ_0 we apply a solvability condition to (3.7). The corresponding homogeneous adjoint problem is

$$L^\dagger\Psi^\dagger = \Psi^{\dagger\prime\prime} + \mathcal{E}^t\Psi^\dagger = 0\,, \tag{3.9}$$

where t denotes transpose. We look for odd solutions for $\Psi_1^\dagger$ and $\Psi_2^\dagger$, with $\Psi_1^\dagger \to 0$ and $\Psi_2^\dagger$ bounded as $|y| \to \infty$.

Multiplying $L\Psi$ by $\Psi^\dagger$, and integrating, we obtain the solvability condition

$$\int_{-\infty}^{\infty}\Psi^{\dagger t}L\Psi\,dy = \lambda_0\int_{-\infty}^{\infty}\Psi_1^\dagger V_0'\,dy + \int_{-\infty}^{\infty}\Psi^{\dagger t}\begin{pmatrix}-2(V_0U_1+U_0V_1) & -2V_0V_1\\ 2(V_0U_1+U_0V_1) & 2V_0V_1\end{pmatrix}\begin{pmatrix}V_0'\\ U_0'\end{pmatrix}dy\,. \tag{3.10}$$

Upon integrating the left-hand side of (3.10) by parts, and using $L^\dagger\Psi^\dagger = 0$, we get

$$\int_{-\infty}^{\infty}\Psi^{\dagger t}L\Psi\,dy = \Psi_2^\dagger(\infty)N_1'(\infty) - \Psi_2^\dagger(-\infty)N_1'(-\infty) = \Psi_2^\dagger(\infty)\left[N_1'(\infty) + N_1'(-\infty)\right]\,. \tag{3.11}$$

Substituting (3.11) into (3.10), we obtain

$$2I_2\lambda_0 = \Psi_2^\dagger(\infty)\left[N_1'(+\infty) + N_1'(-\infty)\right)] - I_1\,, \tag{3.12 a}$$

where I_1 and I_2 are defined by

$$I_2 = \int_0^\infty \Psi_1^\dagger V_0' \, dy \,, \qquad I_1 = \int_{-\infty}^\infty \Psi^{\dagger t} \begin{pmatrix} -2\,(V_0U_0)' & -\left(V_0^2\right)' \\ 2\,(V_0U_0)' & \left(V_0^2\right)' \end{pmatrix} \begin{pmatrix} V_1 \\ U_1 \end{pmatrix} dy \,. \tag{3.12 b}$$

The integral I_1 can be evaluated explicitly by using the equation obtain by differentiating (2.3 b). We calculate,

$$LW = \begin{pmatrix} -2\,(V_0U_0)' & -\left(V_0^2\right)' \\ 2\,(V_0U_0)' & \left(V_0^2\right)' \end{pmatrix} \begin{pmatrix} V_1 \\ U_1 \end{pmatrix}, \qquad W \equiv \begin{pmatrix} V_1' \\ U_1' \end{pmatrix} .$$

Therefore, upon integrating by parts, we can calculate I_1 in (3.12 b) as

$$I_1 = \int_{-\infty}^\infty \Psi^{\dagger t} LW \, dy = \Psi_2^\dagger(+\infty) U_1^{''}(+\infty) - \Psi_2^\dagger(-\infty) U_1^{''}(-\infty) = -2\Psi_2^\dagger(+\infty) \,. \tag{3.13}$$

Here we used $U_1^{''}(\pm\infty) = -1$ from (2.11) and that Ψ_2 is odd. Substituting (3.13) into (3.12 a), we get

$$\lambda_0 = -\alpha \left(\frac{N_1'(+\infty) + N_1'(-\infty)}{2} + 1 \right), \qquad \alpha \equiv \frac{-\Psi_2^\dagger(+\infty)}{\int_0^\infty \Psi_1^\dagger V_0' \, dy} \,. \tag{3.14}$$

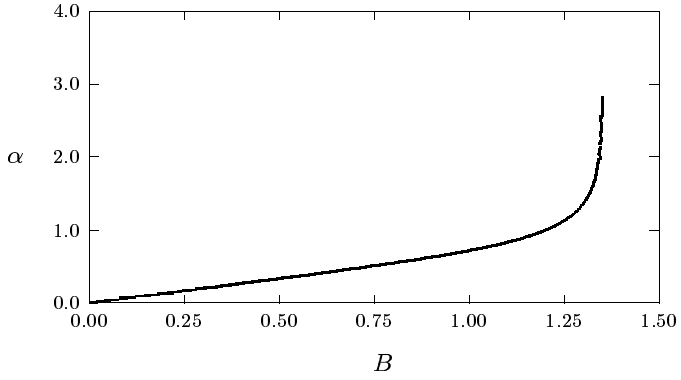

FIGURE 2. Plot of α, defined in (3.24), versus B along the primary solution branch of the γ versus B bifurcation diagram. The right endpoint of this curve corresponds to the fold point $B = 1.347$.

The constant α depends on the core solution through the parameter B of Principal Result 2.1. In Fig. 2 we plot the numerically computed $\alpha = \alpha(B)$ along the primary branch of the $\gamma = \gamma(B)$ curve (cf. [**17**]). This plot shows that $\alpha > 0$. As a partial analytical confirmation of the sign of α, we use Principal Result 2.2 to calculate α in the intermediate regime where $B \sim 3\delta \ll 1$. From this result, (3.9) reduces in the intermediate regime to

$$\psi_{1yy}^\dagger + (-1 + 2w)\psi_1^\dagger \sim 2w\psi_2^\dagger \,, \qquad \psi_{2yy}^\dagger + \delta^2 w^2 \left(\psi_1^\dagger - \psi_2^\dagger \right) \sim 0 \,. \tag{3.15}$$

Therefore, $\psi_1^\dagger = w_y + O(\delta^2)$ and $\psi_2^\dagger = -\frac{\delta^2}{3} \int_0^y [w(s)]^3 \, ds + O(\delta^4)$. Since $V_0 \sim \delta w$ and $w(y) = \frac{3}{2}\mathrm{sech}^2(y/2)$ from Principal Result 2.2, we obtain $\alpha \sim \frac{\delta}{3} \left(\int_0^\infty w^3 \, dy / \int_0^\infty w_y^2 \, dy \right) \sim 2\delta$. Therefore, in the intermediate regime $O(\varepsilon^{1/2}) \ll \delta \ll O(1)$ we have $B \sim 3\delta$ and $\alpha \sim 2\delta$. By using $\delta \sim A/[3\coth(l)]$ and $B = A\tanh(l)$, we obtain

$$\alpha \sim \frac{2A}{3} \tanh(l) \sim \frac{2B}{3} > 0 \,, \qquad \text{for} \quad A \ll 1 \,. \tag{3.16}$$

To determine λ_0 in (3.14), we must calculate $N_1'(\pm\infty)$ by constructing an appropriate outer solution for the eigenpair of (3.2). In the outer region, we obtain from (3.2) that η satisfies

$$\eta_{x_1x_1} - \left(1 + m^2 + \tau\lambda\right)\eta = 2u_e v_e \phi + v_e^2 \eta \quad -l < x_1 < l\,; \qquad \eta_{x_1}(\pm l) = 0\,. \tag{3.17}$$

The right-hand side of (3.17) is localized near $x_1 = 0$, and from (3.3) we find for $x_1 = O(\varepsilon)$ that

$$2u_e v_e \phi + v_e^2 \eta \sim \frac{2}{\varepsilon A}\left(UV\Phi\right) + \frac{1}{\varepsilon A}\left(V^2 N\right)\,. \tag{3.18}$$

By expanding V, U, Φ, and N, in powers of εA as in (2.2) and (3.5), we get that (3.18) becomes

$$2u_e v_e \phi + v_e^2 \eta \sim \frac{1}{\varepsilon A}\left(U_0 V_0^2\right)' + N_1''\,. \tag{3.19}$$

Therefore, since $2B = \int_{-\infty}^{\infty} U_0 V_0^2\, dy$ and $B = A\tanh l$, we obtain in the sense of distributions that η satisfies

$$\eta_{x_1x_1} - \left(1 + m^2 + \tau\lambda\right)\eta = 2\varepsilon\tanh(l)\delta'(x_1) + \varepsilon\left[N_1'(+\infty) - N_1'(-\infty)\right]\delta(x_1)\,, \quad -l < x_1 < l\,, \tag{3.20}$$

with $\eta_{x_1}(\pm l) = 0$. The matching condition of the inner and outer solutions for η requires that

$$\frac{\varepsilon}{A}\left(N_0 + \varepsilon A N_1 + \cdots\right) \sim \eta\left(0^{\pm}\right) + \varepsilon y \eta_{x_1}\left(0^{\pm}\right) + \cdots\,. \tag{3.21}$$

Since $N_0 = U_0'$ satisfies $N_0(\pm\infty) = \pm B$, we get from this matching condition that

$$\eta\left(0^{\pm}\right) = \pm\frac{\varepsilon B}{A} = \pm\varepsilon\tanh(l)\,, \qquad N_1'(\pm\infty) = \varepsilon^{-1}\eta_{x_1}\left(0^{\pm}\right)\,. \tag{3.22}$$

Solving (3.20) for $\eta(x_1)$, we obtain that

$$\eta(x_1) = \varepsilon\tanh l\frac{\cosh\theta(l - x_1)}{\cosh(\theta l)}\,, \quad 0 < x_1 < l\,; \qquad \eta(x_1) = -\varepsilon\tanh l\frac{\cosh\theta(l + x_1)}{\cosh(\theta l)}\,, \quad -l < x_1 < 0\,, \tag{3.23}$$

where θ is defined by $\theta \equiv \sqrt{1 + \tau\lambda + m^2}$. From (3.22) this yields that $N_1'(\pm\infty) = -\theta\tanh(\theta l)\tanh l$. Finally, substituting this formula into (3.14), and using (3.5), we obtain the following result:

Principal Result 3.1: *Consider a stripe equilibrium solution (U_0, V_0) of (1.3) in the high feed-rate and intermediate regimes, as given by Principal Results 2.1 and 2.2, respectively. Suppose that $m = O(1)$ as $\varepsilon \to 0$. Then, in the inner region, any instability of the linearized problem has the form*

$$U \sim U_0\left(y + ce^{imx_2}e^{\lambda t}\right)\,, \qquad V \sim V_0\left(y + ce^{imx_2}e^{\lambda t}\right)\,,$$

where $y = \varepsilon^{-1}x_1$, c is a small constant, and λ satisfies the transcendental equation

$$\lambda \sim -\varepsilon A\alpha\left(1 - \theta\tanh(\theta l)\tanh l\right)\,, \qquad \theta \equiv \sqrt{1 + \lambda\tau + m^2}\,, \qquad \alpha \equiv \frac{-\Psi_2^{\dagger}(+\infty)}{\int_0^{\infty}\Psi_1^{\dagger}V_0'\, dy}\,. \tag{3.24}$$

Here $\alpha > 0$ along the primary branch of the $\gamma = \gamma(B)$ curve. Since $\lambda = O(\varepsilon)$, then $\theta \sim \sqrt{1 + m^2}$ when $\tau = O(1)$. Thus, for $\tau = O(1)$, the stripe solution is unstable for $m > m_{zs}$, where m_{zs} is the unique root of

$$\sqrt{1 + m^2}\tanh l\tanh\left(l\sqrt{1 + m^2}\right) = 1\,. \tag{3.25}$$

In Fig. 3 we plot the domain half-length l versus m_{zs}. It is clear that $m_{zs} \to 0$ as $l \to \infty$. Additionally, it easy to see that $m_{zs} \sim \omega/l$ as $l \to 0$, where $\omega = 1.1997$ is the unique root of $\omega\tanh\omega = 1$.

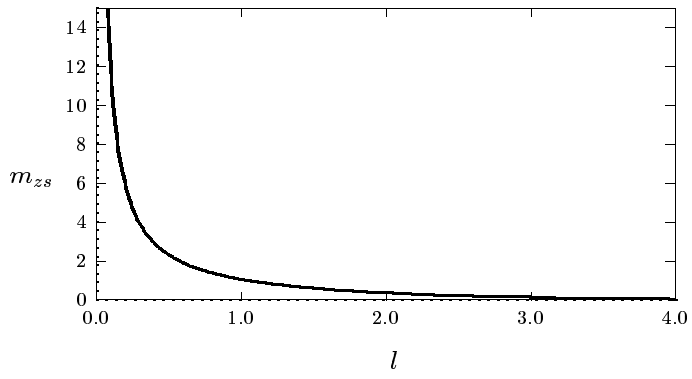

FIGURE 3. Plot of the smallest unstable mode m_{zs} versus the domain half-length l obtained from (3.25).

To determine if the stripe is re-stabilized when m is asymptotically large as $\varepsilon \to 0$, we must consider two distinguished ranges of m: $O(1) \ll m \ll O(\varepsilon^{-1})$, and $m = O(\varepsilon^{-1})$. On the range $O(1) \ll m \ll O(\varepsilon^{-1})$, we now show that the stripe is still unstable. In the inner region, we expand the solution to (3.4) as

$$\Phi = V_0^{'} + \varepsilon m \Phi_1 + \cdots , \quad N = U_0^{'} + \varepsilon m N_1 + \cdots , \quad \lambda = \varepsilon m \lambda_0 + \cdots . \tag{3.26}$$

Substituting (3.26) and (2.2) into (3.4), and assuming that $m \gg 1$, we collect terms proportional to εm to get

$$\Phi_1'' - \Phi_1 + V_0^2 N_1 + 2V_0 U_0 \Phi_1 = \lambda_0 V_0^{'} , \qquad N_1'' - V_0^2 N_1 - 2V_0 U_0 \Phi_1 = 0 , \qquad -\infty < y < \infty . \tag{3.27}$$

To determine λ_0, we multiply (3.27) by the adjoint solution $\Psi^{\dagger}$ of (3.9). Integrating over the domain, we get

$$\int_{-\infty}^{\infty} \Psi^{\dagger t} L \Psi \, dy = \Psi_2^{\dagger}(\infty) \left[N_1^{'}(\infty) + N_1^{'}(-\infty) \right] = \lambda_0 \int_{-\infty}^{\infty} \Psi_1^{\dagger} V_0^{'} \, dy . \tag{3.28}$$

To determine $N_1^{'}(\pm\infty)$, we proceed as in the analysis of (3.17)–(3.19). Since $m \gg O(1)$, we obtain on either side of the stripe location $x_1 = 0$ that the outer solution for η asymptotically satisfies

$$\eta_{x_1 x_1} - m^2 \eta = 0 , \quad -l < x_1 < l ; \qquad \eta_{x_1}(\pm l) = 0 . \tag{3.29}$$

The matching condition for the inner and outer solutions for η is that

$$\frac{\varepsilon}{A} \left(U_0^{'}(\pm\infty) + \varepsilon m N_1 + \cdots \right) \sim \eta \left(0^{\pm} \right) + \varepsilon y \eta_{x_1} \left(0^{\pm} \right) + \cdots . \tag{3.30}$$

Since $U_0^{'}(\pm\infty) = \pm B$, this condition yields that $\eta(0^{\pm}) = \pm \varepsilon B / A = \pm \varepsilon \tanh l$, and $N_1^{'}(\pm\infty) = \frac{A}{\varepsilon m} \eta_{x_1}(0^{\pm})$. Therefore, the solution to (3.29) is $\eta(x_1) \sim \mathrm{sign}(x_1)(\varepsilon \tanh l) e^{-m|x_1|}$. This yields $N_1^{'}(\pm\infty) = -A \tanh l$, which determines λ_0 from (3.28). In this way, we calculate

$$\lambda \sim \varepsilon m \alpha A \tanh l , \tag{3.31}$$

which is valid for $O(1) \ll m \ll O(\varepsilon^{-1})$ and $A = O(1)$. Since $\alpha > 0$ along the primary branch of the $\gamma = \gamma(B)$ curve, we conclude that all of these modes are unstable along this branch due to a real positive eigenvalue. As a remark, (3.31) can also be obtained formally by letting $m \to \infty$ in (3.24) of Principal Result 3.1.

To determine the re-stabilization threshold for the zigzag instability of a stripe in the high feed-rate regime $A = O(1)$, we must consider the regime $m = O(\varepsilon^{-1})$. Thus, we introduce m_0 by $m = m_0\varepsilon^{-1}$, where $m_0 = O(1)$. From (3.4), the corresponding leading-order eigenvalue problem, defined on $-\infty < y < \infty$, is

$$(\lambda + m_0^2)\Phi_0 = \Phi_0'' - \Phi_0 + V_0^2 N_0 + 2V_0U_0\Phi_0\,, \qquad m_0^2 N_0 = N_0'' - V_0^2 N_0 - 2V_0U_0\Phi_0\,. \tag{3.32}$$

We seek an odd eigenfunction to this problem for which $\Phi_0 \to 0$ $y \to \pm\infty$. For this range of m, the outer solution for η is exponentially small, and so the matching condition is simply that $N_0 \to 0$ as $y \to \pm\infty$.

In the high feed-rate regime (3.32) can only be solved numerically. To do so, we discretize (3.32) on a long interval $[0, L]$ using centered finite differences, ensuring that Φ_0 and N_0 are odd functions so that $N_0(0) = \Phi_0(0) = 0$. We choose a meshsize $h = L/n$, where $n > 1$, and label $y_1 = h$ and $y_n = L$. This leads to

$$\left(\mathcal{M} - \left(1 + m_0^2\right) I + \Lambda_2\right) \boldsymbol{\Phi_0} + \Lambda_1 \boldsymbol{N_0} = \lambda \boldsymbol{\Phi_0}\,, \qquad \left(\mathcal{M} - m_0^2 I - \Lambda_1\right) \boldsymbol{N_0} = \Lambda_2 \boldsymbol{\Phi_0}\,. \tag{3.33 a}$$

By eliminating $\boldsymbol{N_0}$, we obtain the discrete eigenvalue problem

$$\left(\mathcal{M} - \left(1 + m_0^2\right) I + \Lambda_2 + \Lambda_1 \left(\mathcal{M} - m_0^2 I - \Lambda_1\right)^{-1} \Lambda_2\right) \boldsymbol{\Phi_0} = \lambda \boldsymbol{\Phi_0}\,. \tag{3.33 b}$$

Here $\boldsymbol{\Phi_0} = (\Phi_0(y_1), \ldots, \Phi_0(y_n))^t$ and $\boldsymbol{N_0} = (N_0(y_1), \ldots, N_0(y_n))^t$. In addition, Λ_1 and Λ_2 are $n \times n$ diagonal matrices, and $\mathcal{M}$ is a tridiagonal matrix of the same size. These matrices have the form

$$\Lambda_{1ii} = V_0^2(y_i)\,, \qquad \Lambda_{2ii} = 2U_0(y_i)V_0(y_i)\,, \qquad \mathcal{M} \equiv \frac{1}{h^2}\begin{pmatrix} -2 & 1 & 0 & \cdots & 0 & 0 & 0 \\ 1 & -2 & 1 & \ddots & \ddots & 0 & 0 \\ 0 & \ddots & \ddots & \ddots & \ddots & \ddots & 0 \\ \vdots & \ddots & \ddots & \ddots & \ddots & \ddots & \vdots \\ 0 & \ddots & \ddots & \ddots & \ddots & \ddots & 0 \\ 0 & 0 & \ddots & \ddots & 1 & -2 & 1 \\ 0 & 0 & 0 & \cdots & 0 & 2 & -2 \end{pmatrix}. \tag{3.34}$$

Our computational results show that there is a critical value m_{0z} of m_0 for which $\mathrm{Re}(\lambda) < 0$ for $m_0 > m_{0z}$ and $\mathrm{Re}(\lambda) > 0$ for $m_0 < m_{0z}$. This re-stabilization value m_{0z} is computed numerically from the discrete eigenvalue problem (3.33 *b*) using LAPACK [**1**] on a domain with $L = 12$ and $n = 200$ meshpoints. Increasing the number of meshpoints and the domain length did not change the results significantly. In Fig. 4(a) we plot the critical mode m_{0z}, corresponding to $\lambda = 0$, at each point along the primary branch of the γ versus B bifurcation diagram. Our computational results also show that there is exactly one unstable eigenvalue λ_0 below the re-stabilization threshold and that this eigenvalue is real. In Fig. 4(b) we plot λ_0 versus εm below the stability threshold for four values of B. Notice that the critical mode m_{0z} tends to zero as $\gamma \to 1.5$ (and consequently $B \to 0$). Therefore, this suggests the re-stabilization value of m in the intermediate regime is no longer $O(\varepsilon^{-1})$. Numerical results for m_{0z} for various values of B are given in the last column of Table 1.

Fig. 4(a) suggests that all of the modes with $m = O(\varepsilon^{-1})$ should be stable in the intermediate regime $O(\varepsilon^{1/2}) \ll A \ll O(1)$. We now show this analytically by using the limiting form of V_0 and U_0 in this regime as

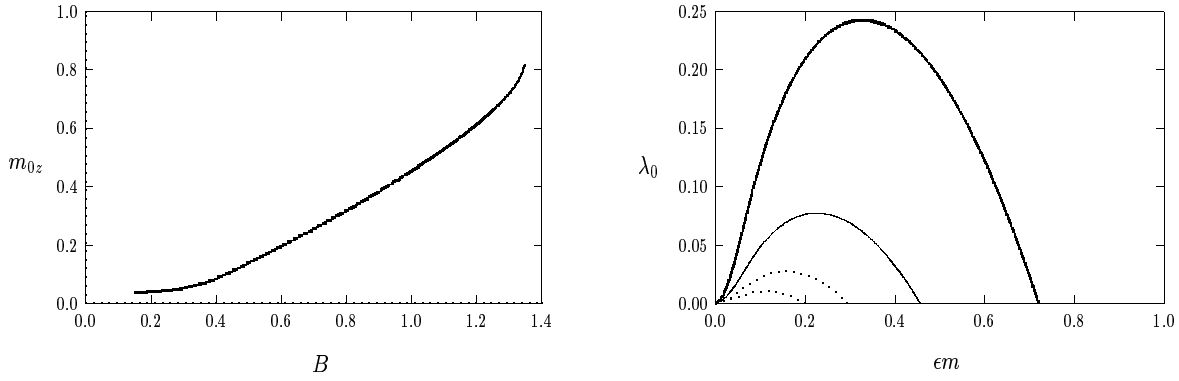

(a) m_{0z} versus B (b) λ_0 versus εm

FIGURE 4. Left figure: plot of the re-stabilization value m_{0z} (with $m = \varepsilon^{-1} m_{0z}$) versus B, computed from (3.32), along the primary branch of the $\gamma(B)$ curve. Above this curve we regain stability with respect to zigzag perturbations. Right figure: plot of the largest eigenvalue λ_0 versus εm below the stability threshold for $B = 0.594$ (widely spaced dots), $B = 0.761$ (dotted curve), $B = 1.00$ (solid curve), and $B = 1.3$ (heavy solid curve).

given in Principal Result 2.2. From (2.18) we calculate

$$V_0^2 = \delta^2 w^2 + 2\delta^4 w v_1 + \cdots , \qquad U_0 V_0 = w + \delta^2 (v_1 + u_1 w) + \cdots . \tag{3.35}$$

By substituting (3.35) into (3.32), a dominant balance argument suggests that we should expand

$$\Phi_0 = \Phi_{00} + \delta^2 \Phi_{01} + \cdots , \qquad N_0 = N_{00} + \delta^2 N_{01} + \cdots , \qquad m_0 = \delta\mu + \cdots , \qquad \lambda = \lambda_0 \delta^2 + \cdots . \tag{3.36}$$

Substituting (3.35) and (3.36) into (3.32), and collecting terms of $O(\delta^2)$, we get

$$L_0 \Phi_{00} \equiv \Phi_{00}'' - \Phi_{00} + 2w\Phi_{00} = 0 ; \qquad N_{00}'' = 2w\Phi_{00} , \tag{3.37 a}$$

$$L_0 \Phi_{01} = \left(\lambda_0 + \mu^2\right) \Phi_{00} - w^2 N_{00} - 2(v_1 + u_1 w)\Phi_{00} . \tag{3.37 b}$$

Comparing (3.37 a) with (2.19) and (2.20), we conclude that $\Phi_{00} = w'$ and $N_{00} = u_1'$, where $w(y) = \frac{3}{2}\mathrm{sech}^2(y/2)$ and u_1 satisfies (2.20). Since $L_0 w' = 0$, the solvability condition for (3.37 b) yields that

$$\left(\lambda_0 + \mu^2\right) \int_{-\infty}^{\infty} w'^2 \, dy = \int_{-\infty}^{\infty} w^2 w' u_1' \, dy + 2 \int_{-\infty}^{\infty} (u_1 w + v_1) \, w'^2 \, dy . \tag{3.38}$$

To simplify (3.38) we differentiate the equation (2.20) for v_1 to get $L_0 v_1' = -w^2 u_1' - 2(v_1 + u_1 w)w'$. Since $L_0 w' = 0$, the solvability condition for $L_0 v_1'$ readily yields that the right hand-side of (3.38) is identically zero. Therefore, (3.38) reduces to $\lambda_0 = -\mu^2$. From (3.36) we get $\lambda \sim -\delta^2 \mu^2$ and $m = \delta\mu/\varepsilon$, which implies that

$$\lambda \sim -(\varepsilon m)^2 . \tag{3.39}$$

This shows that all of the modes with $m = O(\delta/\varepsilon) \ll O(\varepsilon^{-1})$ are stable in the intermediate regime.

To determine the re-stabilization threshold in the intermediate regime we must return to (3.27). Notice that

(3.27) is not uniformly valid in the intermediate since we have neglected the term $\varepsilon^2 m^2 \Phi$ in (3.4). This is seen by comparing the terms εA with $\varepsilon^2 m^2$ in this regime. In this regime, we get from Principal Result 2.2 that $A = O(\delta)$ with $O(\varepsilon^{1/2}) \ll \delta \ll 1$. Therefore, when $m = O\left(\delta^2/\varepsilon\right)$, we conclude that $\varepsilon^2 m^2 \gg \varepsilon A$ when $\delta \gg O(\varepsilon^{1/3})$, and $\varepsilon^2 m^2 \ll \varepsilon A$ when $O(\varepsilon^{1/2}) \ll \delta \ll O(\varepsilon^{1/3})$. Therefore, we must include the term $\varepsilon^2 m^2 \Phi$ in the analysis. Formally re-writing (3.27), but now including the term $\varepsilon^2 m^2 \Phi_0$, we obtain

$$\Phi_1'' - \Phi_1 + V_0^2 N_1 + 2V_0 U_0 \Phi_1 = (\lambda_0 + m\varepsilon)\, V_0' \,, \tag{3.40}$$

This shows that we need only replace λ_0 with $\lambda_0 + m\varepsilon$. Then, proceeding as in the derivation of (3.31), we obtain that $\lambda_0 \sim -\varepsilon m + \alpha A \tanh l$. From Principal Result 2.2 and (3.16), we recall that $B = A \tanh l \sim 3\delta$ and $\alpha \sim 2\delta$ in the intermediate regime. Therefore, with $\lambda = \varepsilon m \lambda_0$, this expression of λ_0 becomes

$$\lambda \sim \varepsilon m \left(6\delta^2 - \varepsilon m\right) \,. \tag{3.41}$$

Equation (3.41) shows that the re-stabilization threshold in the intermediate regime occurs when $m \sim 6\delta^2/\varepsilon$, or equivalently $m_{0z} \sim 6\delta^2$. Notice that when $m = O(\varepsilon^{-1})$, (3.41) reduces asymptotically to (3.39). We summarize our main result for zigzag instabilities of a stripe as follows:

Principal Result 3.2: *Consider a stripe equilibrium solution (U_0, V_0) of (1.3). Suppose that $\varepsilon \ll 1$ and $\tau = O(1)$. Then, all zigzag-type perturbations of the form $U \sim U_0(y) + ce^{imx_2} e^{\lambda t}\phi$ and $V \sim V_0(y) + ce^{imx_2} e^{\lambda t}\eta$, with $y = x_1/\varepsilon$, are unstable only in the zone $m_{zs} < m < \varepsilon^{-1} m_{0z}$. Here m_{zs} is the root of (3.25), which depends only on the domain half-length l. In the high-feed rate regime, the re-stabilization threshold m_{0z}, plotted in Fig. 4(a), depends on the specific point along the primary branch of the $\gamma = \gamma(B)$ curve. Here B is related to l and A by $B = A \tanh l$. In the intermediate regime $O(\varepsilon^{1/2}) \ll A \ll O(1)$, the re-stabilization threshold is $m_{0z} \sim \frac{2}{3} A^2 \tanh^2(l)$.*

As a remark, in all of the analysis in this section we have assumed that $\tau = O(1)$ as $\varepsilon \to 0$. If we were to allow $\tau = O(\varepsilon^{-1})$, then for each fixed value of m we could get a zigzag instability due a Hopf bifurcation when τ is increased past some threshold. This type of Hopf bifurcation was studied in §4 of [**17**] for a one-dimensional spike solution corresponding to $m = 0$. We will not consider the case of asymptotically large τ here.

4 Breakup Instabilities of a Stripe

We now study the stability, with respect to the large eigenvalues, of the stripe equilibrium solution constructed in §2. These instabilities, referred to as breakup instabilities, are the mechanism by which a stripe breaks up into a sequence of spots. As in §3, we look for a normal mode solution in the inner region in the form

$$v = \frac{1}{\varepsilon}\left(V(y) + e^{\lambda t} e^{imx_2} \Phi(y)\right) \,, \qquad u = \frac{\varepsilon}{A}\left(U(y) + e^{\lambda t} e^{imx_2} N(y)\right) \,, \qquad y = \varepsilon^{-1} x_1 \,, \tag{4.1}$$

where U, V, Φ, and N, are expanded in powers of εA. In contrast to the study of the small eigenvalues in §3, we now look for even functions Φ and N. Substituting (4.1) into (1.3), assuming that $\tau = O(1)$, and defining μ by $\mu \equiv \varepsilon^2 m^2$, we obtain the following leading-order eigenvalue problem on $-\infty < y < \infty$:

$$\lambda \Phi_0 = \Phi_0'' - (1+\mu)\,\Phi_0 + V_0^2 N_0 + 2V_0 U_0 \Phi_0 \,, \qquad N_0'' - \mu N_0 - V_0^2 N_0 - 2V_0 U_0 \Phi_0 = 0 \,, \qquad \mu \equiv \varepsilon^2 m^2 \,. \tag{4.2}$$

To determine the instability band for (4.2), we discretize (4.2) on a long interval $[0, L]$ using centered finite differences and ensuring that Φ_0 and N_0 are even functions. The resulting discrete eigenvalue problem is similar to (3.33), except for slight differences in the matrix structure due to the different parity of the breakup eigenfunction. Our computational results, obtained from LAPACK [**1**] with $n = 200$ meshpoints and $L = 12$, show that there are threshold values μ_1 and μ_2 for which $\mathrm{Re}(\lambda) > 0$ for $\sqrt{\mu_1} < \varepsilon m < \sqrt{\mu_2}$, and $\mathrm{Re}(\lambda) < 0$ for $0 \le \varepsilon m < \sqrt{\mu_1}$ and $\varepsilon m > \sqrt{\mu_2}$. Increasing n and L did not change the results significantly. Our computational results show that there is exactly one unstable eigenvalue λ_0 between the stability thresholds and that this eigenvalue is real. In Fig. 5(a) and in Table 1, we give numerical results for $\sqrt{\mu_1}$ and $\sqrt{\mu_2}$ versus B along the primary branch of the $\gamma = \gamma(B)$ curve associated with the core problem. In Fig. 5(b) we plot λ_0 versus εm between the stability thresholds for four values of B, where B is related to A and l by $B = A \tanh l$.

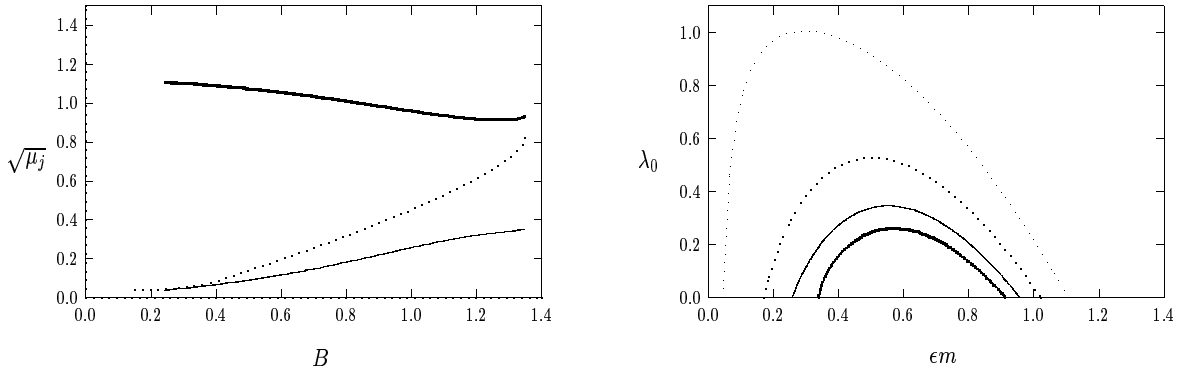

(a) $\sqrt{\mu_j}$ versus B (b) λ_0 versus εm

FIGURE 5. Left figure: plots of $\sqrt{\mu_1}$ (heavy solid curve) and $\sqrt{\mu_2}$ (solid curve) versus B computed from (4.2) along the primary branch of the $\gamma = \gamma(B)$ curve associated with the core problem. Between these curves we have breakup instabilities. The threshold modes are $m_j = \sqrt{\mu_j}/\varepsilon$ for $j = 1, 2$. The zigzag threshold m_{0z} versus B (dotted curve) is also plotted. Right figure: plot of the largest eigenvalue λ_0 versus εm between the stability thresholds for $B = 0.285$ (widely spaced dots), $B = 0.761$ (dotted curve), $B = 1.00$ (solid curve), and $B = 1.3$ (heavy solid curve).

Although we are unable to calculate μ_1 and μ_2 analytically in the high feed-rate regime, we can asymptotically calculate these thresholds where $\lambda = 0$ in the intermediate regime where $B = 3\delta \ll 1$ with $O(\varepsilon^{1/2}) \ll \delta \ll O(1)$. In the intermediate regime we use Principal Result 2.2 for V_0 and U_0. In this way, (4.2) reduces to

$$(\mu + \lambda)\Phi_0 \sim \Phi_0'' - \Phi_0 + 2\left(w + O(\delta^2)\right)\Phi_0 + \left(\delta^2 w^2 + O(\delta^4)\right) N_0\,, \tag{4.3 a}$$

$$\mu N_0 \sim N_0'' - 2\left(w + O(\delta^2)\right)\Phi_0 - \left(\delta^2 w^2 + O(\delta^4)\right) N_0\,. \tag{4.3 b}$$

The balance of the various terms in the first equation gives rise to two possibilities: either $O(N_0)\delta^2 \ll O(\Phi_0)$ or $O(N_0)\delta^2 = O(\Phi_0)$. In the former case, Φ_0 satisfies the well-known Fisher eigenvalue problem (cf. [**25**])

$$(\mu + \lambda)\Phi_0 = \Phi_0'' - \Phi_0 + 2w\Phi_0\,, \qquad -\infty < y < \infty\,; \qquad \Phi_0 \to 0 \quad \text{as} \quad y \to \pm\infty\,, \tag{4.4}$$

γ	B	$\sqrt{\mu_1}$	$\sqrt{\mu_2}$	m_{0z} (zigzag)
1.470	0.361	0.059	1.095	0.086
1.443	0.501	0.089	1.074	0.149
1.416	0.611	0.120	1.053	0.207
1.388	0.704	0.149	1.033	0.260
1.357	0.800	0.183	1.010	0.319
1.316	0.909	0.223	0.983	0.390
1.275	1.005	0.259	0.958	0.457
1.216	1.126	0.300	0.931	0.549
1.138	1.253	0.332	0.913	0.664
1.097	1.300	0.339	0.914	0.719
1.020	1.347	0.351	0.934	0.820

Table 1. The thresholds $\sqrt{\mu_1}$ and $\sqrt{\mu_2}$ of Principal Result 4.2 for breakup instabilities, together with the upper threshold m_{0z} for zigzag instabilities, along the primary branch of the $\gamma = \gamma(B)$ curve of the core problem.

which has a unique positive eigenvalue $\mu + \lambda = \frac{5}{4}$. This gives the upper bound $\mu_2 = \frac{5}{4}$ for the instability band. The result $\sqrt{\mu_2} = \frac{\sqrt{5}}{2} \approx 1.12$ is the limiting value of the heavy solid curve seen in Fig. 5(a) for $B \ll 1$.

For the second possibility, a dominant balance argument suggest that

$$N_0 = \frac{1}{\delta^2}\left(N_{00} + \delta^2 N_{01} + \cdots\right), \qquad \mu = \delta^2\mu_0 + \cdots, \qquad \Phi_0 = \Phi_{00} + \delta^2\Phi_{01} + \cdots. \tag{4.5}$$

Substituting (4.5) into (4.3), we get $N_{00}'' = 0$,. Thus, N_{00} an unknown constant. In addition, Φ_{00} satisfies

$$\lambda\Phi_{00} = \Phi_{00}'' - \Phi_{00} + 2w\Phi_{00} + N_{00}w^2, \qquad -\infty < y < \infty; \qquad \Phi_{00} \to 0 \quad \text{as} \quad |y| \to \infty. \tag{4.6}$$

To determine N_{00} we must consider the outer region. In this region, we obtain from (3.2) that η satisfies

$$\eta_{x_1x_1} - \left(1 + m^2 + \tau\lambda\right)\eta = 2u_e v_e\phi + v_e^2\eta, \tag{4.7}$$

with $\eta_{x_1}(\pm l) = 0$. The right-hand side of (4.7) is localized near $x_1 = 0$. By using Principal Result 2.2, we calculate

$$2u_e v_e\phi + v_e^2\eta \sim \frac{2w}{\varepsilon A}\Phi_{00} + \frac{w^2}{\varepsilon A}N_{00}. \tag{4.8}$$

Therefore, we obtain the following problem for $\eta(x_1)$:

$$\eta_{x_1x_1} - \left(1 + m^2 + \tau\lambda\right)\eta = \left(\frac{2}{A}\int_{-\infty}^{\infty} w\Phi_{00}\,dy + \frac{N_{00}}{A}\int_{-\infty}^{\infty} w^2\,dy\right)\delta(x_1), \qquad -l < x_1 < l, \tag{4.9}$$

with $\eta_{x_1}(\pm l) = 0$. The solution for η is

$$\eta(x_1) = -\left(\frac{2}{A}\int_{-\infty}^{\infty} w\Phi_{00}\,dy + \frac{N_{00}}{A}\int_{-\infty}^{\infty} w^2\,dy\right)G_m(x_1), \tag{4.10}$$

where $G_m(x_1)$ is the Green's function satisfying

$$G_{mx_1x_1} - \theta^2 G_m = -\delta(x_1), \quad -l < x_1 < l; \qquad G_{mx_1}(\pm l) = 0. \tag{4.11}$$

Here $\theta \equiv \sqrt{1 + m^2 + \tau\lambda}$. The matching condition for the inner and outer solutions is that $\eta(0) = \varepsilon\delta^{-2}N_{00}/A$.

By solving (4.11), and setting $x_1 = 0$ in (4.10), we calculate N_{00} as

$$N_{00}\left(\frac{G_m(0)}{A}\int_{-\infty}^{\infty} w^2\,dy + \frac{\varepsilon}{A\delta^2}\right) = -\frac{2}{A}\left(\int_{-\infty}^{\infty} w\Phi_{00}\,dy\right) G_m(0)\,. \tag{4.12}$$

By calculating the solution to (4.11), we evaluate $G_m(0)$ as

$$G_m(0) = \frac{\coth(l\theta)}{2\theta}\,, \qquad \theta \equiv \sqrt{1+m^2+\tau\lambda}\,. \tag{4.13}$$

By combining (4.12) and (4.6), and using $\int_{-\infty}^{\infty} w^2\,dy = 6$, we obtain the nonlocal eigenvalue problem

$$\Phi_{00}'' - \Phi_{00} + 2w\Phi_{00} - \chi w^2\frac{\int_{-\infty}^{\infty} w\Phi_{00}\,dy}{\int_{-\infty}^{\infty} w^2\,dy} = \lambda\Phi_{00}\,, \quad \Phi_{00}\to 0 \quad \text{as} \quad |y|\to\infty\,; \quad \chi \equiv 2\left[1+\frac{\varepsilon}{6\delta^2 G_m(0)}\right]^{-1}\,. \tag{4.14}$$

To study this problem, defined on $-\infty < y < \infty$, we need the following key stability result of [**43**]:

Lemma 4.1: *(cf. [**43**]). Let $\chi \geq 0$, and consider the nonlocal eigenvalue problem (NLEP)*

$$\Phi'' - \Phi + 2w\Phi - \chi w^2\frac{\int_{-\infty}^{\infty} w\Phi\,dy}{\int_{-\infty}^{\infty} w^2\,dy} = \lambda\Phi\,, \qquad -\infty < y < \infty\,,$$

with $\Phi\to 0$ as $|y|\to\infty$. Then, there are eigenvalues with $Re(\lambda) > 0$ if and only if $\chi < 1$.

We now use this lemma to determine the lower limit of the stability band. In the intermediate regime we have that $\delta \gg O(\varepsilon^{1/2})$. Therefore, if $m = O(1)$, we get from χ in (4.14) that $\chi \sim 2$. Therefore, from Lemma 4.1, we conclude that all the modes with $m = O(1)$ are stable. Alternatively, when $m \gg 1$, we calculate from (4.13) that $G_m(0) \sim [2m]^{-1}$. Therefore, from (4.14), we obtain that $\chi \sim 2\left[1 + m\varepsilon/(3\delta^2)\right]^{-1}$. The stability threshold $\chi = 1$ from Lemma 4.1 is achieved when $m\varepsilon = 3\delta^2$. This yields the lower limit μ_1 of the instability band in the intermediate regime. We summarize our main results for breakup instabilities of a stripe as follows:

Principal Result 4.2: *Let $\varepsilon\to 0$ and $\tau = O(1)$. In the intermediate regime $B = 3\delta \ll 1$, with $B = A\tanh l$, the stripe equilibrium solution of Principal Result 2.2 is unstable to breakup instabilities if and only if*

$$3\delta^2 = \frac{A^2}{3}\tanh^2(l) < \varepsilon m < \frac{\sqrt{5}}{2}\,. \tag{4.15}$$

In the high feed-rate regime, the instability band along the primary solution branch of the $\gamma = \gamma(B)$ curve is

$$\sqrt{\mu_1} < \varepsilon m < \sqrt{\mu_2}\,, \tag{4.16}$$

where $\mu_1 = \mu_1(B)$ and $\mu_2 = \mu_2(B)$ are given in Fig. 5(a) and in Table 1 in terms of the specific point B, with $B = A\tanh l$, along the primary branch associated with the core problem.

5 Equilibria and Stability of a Ring Solution

In this section we modify the methods of §2–4 to obtain analogous results for the stability of an equilibrium ring solution for the GS model (1.3) in the disk domain $\Omega = \{x : |x| \equiv \rho < R\}$. For the high feed-rate regime $A = O(1)$, we begin by constructing an equilibrium ring solution centered at $\rho = \rho_0$, for some ρ_0 with $0 < \rho_0 < R$ to be determined. Although such a solution was constructed in [**22**], we briefly outline the derivation here as many of the formulae are needed for the stability analysis.

In the inner region near ρ_0, we proceed as in §2 by looking for a solution of the form

$$v = \frac{V}{\varepsilon}\,, \qquad u = \frac{\varepsilon U}{A}\,, \qquad r = \varepsilon^{-1}(\rho - \rho_0)\,. \tag{5.1}$$

Substituting (5.1) into (1.3), we obtain on $-\infty < r < \infty$ that

$$V'' + \frac{\varepsilon}{\rho_0 + \varepsilon r}V' - V + V^2 U = 0\,, \qquad U'' + \frac{\varepsilon}{\rho_0 + \varepsilon r}U' - \varepsilon^2 U + A\varepsilon - V^2 U = 0\,. \tag{5.2}$$

Therefore, we expand V and U in a powers of εA as in (2.2) to get that U_0, V_0 satisfy (2.3 a), and that

$$V_1'' - V_1 + 2V_0U_0V_1 + V_0^2U_1 = -\frac{V_0'}{A\rho_0}\,, \qquad U_1'' + 1 - 2V_0U_0V_1 - V_0^2U_1 = -\frac{U_0'}{A\rho_0}\,. \tag{5.3}$$

The asymptotic boundary conditions for U_1 as $r \to \pm\infty$ are to be obtained by matching.

Next, we consider the outer region defined away from ρ_0. By calculating uv^2 in the sense of distributions as in (2.4) of §2, we obtain the following outer problem for $u(\rho)$ in place of (2.5):

$$u_{\rho\rho} + \frac{1}{\rho}u_\rho + 1 - u = C_0\delta(\rho - \rho_0) + \varepsilon C_1\delta(\rho - \rho_0) + \cdots\,, \quad 0 < \rho < R\,; \quad u_\rho(R) = u_\rho(0) = 0\,. \tag{5.4}$$

Here C_0 and C_1 are defined in (2.4) of §2. Therefore, we obtain the two-term outer expansion

$$u = 1 - C_0G(\rho;\rho_0) - \varepsilon C_1G(\rho;\rho_0) + \cdots\,, \tag{5.5}$$

where $G(\rho;\rho_0)$ is the radially symmetric Green's function satisfying

$$G_{\rho\rho} + \frac{1}{\rho}G_\rho - G = -\delta(\rho - \rho_0)\,, \quad 0 < \rho < R\,; \qquad G_\rho(R;\rho_0) = G_\rho(0;\rho_0) = 0\,. \tag{5.6}$$

A simple calculation shows that G is related to the modified Bessel functions I_0 and K_0 by

$$G(\rho,\rho_0) = \rho_0 \begin{cases} J_1(\rho)J_2(\rho_0)\,, & \text{for} \quad 0 < \rho < \rho_0\,, \\ J_1(\rho_0)J_2(\rho)\,, & \text{for} \quad \rho_0 < \rho < R\,, \end{cases} \quad ; \qquad J_1(\rho) \equiv I_0(\rho)\,, \quad J_2(\rho) \equiv K_0(\rho) - \frac{K_0'(R)}{I_0'(R)}I_0(\rho)\,. \tag{5.7}$$

The matching condition between the inner and outer solution is that

$$\begin{aligned} \frac{\varepsilon}{A}\left(U_0(r) + A\varepsilon U_1(r) + \cdots\right) \sim 1 - C_0G(\rho_0,\rho_0) - \left(C_0G_\rho(\rho_0^\pm;\rho_0)r + C_1G(\rho_0;\rho_0)\right)\varepsilon \\ - \left(\frac{r^2}{2}C_0G_{\rho\rho}(\rho_0^\pm;\rho_0) + C_1rG_\rho(\rho_0^\pm;\rho_0)\right)\varepsilon^2 + \cdots\,. \end{aligned} \tag{5.8}$$

The leading-order matching condition yields $C_0G(\rho_0;\rho_0) = 1$. By using (2.4), this yields that

$$B \equiv \int_0^\infty U_0V_0^2\,dr = \frac{A}{2G(\rho_0;\rho_0)}\,. \tag{5.9}$$

From (5.8) we obtain the far-field condition for U_0

$$U_0 \sim -\frac{AG_\rho(\rho_0^\pm;\rho_0)}{G(\rho_0;\rho_0)}r\,, \quad \text{as} \quad r \to \pm\infty\,. \tag{5.10}$$

By applying a solvability condition to (5.3), it follows that the equilibrium ring radius ρ_0 is such that U_0 and V_0 are even functions (cf. [**22**]). This implies that $U_0'(+\infty) = -U_0'(-\infty)$, which yields $G_\rho(\rho_0^+,\rho_0) = -G_\rho(\rho_0^-,\rho_0)$ from (5.10). Therefore, from (5.7), it follows that ρ_0 satisfies the transcendental equation

$$[J_1(\rho)J_2(\rho)]'\,|_{\rho=\rho_0} = 0\,. \tag{5.11}$$

It was shown in Lemma 3.4 of [**22**] that there is a root ρ_0 to (5.11) with $0 < \rho_0 < R$.

Since, in addition, $G_\rho(\rho_0^+, \rho_0) - G_\rho(\rho_0^-, \rho_0) = -1$, we get that $G_\rho(\rho_0^\pm; \rho_0) = \mp 1/2$. Therefore, from (5.10), U_0 has the asymptotic behavior $U_0 \sim B|r|$ as $r \to \pm\infty$, where B is given in (5.9). This shows that U_0 and V_0 satisfy the same core problem as for the stripe equilibrium solution in §2. A two-term far-field expansion for U_0 is then given in (2.10). Substituting (2.10) into (5.8), we obtain the far-field form for U_1 given by $U_1 \sim -\frac{r^2}{2} - \frac{Er}{4}[G(\rho_0;\rho_0)]^{-2}$ as $r \to \pm\infty$, where E is defined in (2.10). The result is summarized as follows:

Principal Result 5.1: *(cf. [**22**]). Let $\Omega = \{x : |x| \equiv \rho < R\}$, and define B by*

$$B = \frac{A}{2G(\rho_0;\rho_0)} = \frac{A}{2\rho_0 J_1(\rho_0) J_2(\rho_0)}\,. \tag{5.12}$$

Here ρ_0 is a root of (5.11), and J_1 and J_2 are defined in (5.7). Suppose that $A = O(1)$ and $B < 1.347$. Then, along the primary branch of the $\gamma = \gamma(B)$ curve associated with the core problem of §2, there exists an equilibrium ring solution to (1.3) of the form

$$v_e \sim \frac{1}{\varepsilon}\left(V_0(r) + \cdots\right) \qquad u_e \sim \frac{\varepsilon}{A}\left(U_0(r) + \cdots\right)\,, \qquad r = \varepsilon^{-1}(\rho - \rho_0)\,. \tag{5.13}$$

Here $V_0(y)$, $U_0(y)$ are even solutions to (2.3 a) subject to $V_0 \to 0$ and $U_0' \to B$ as $r \to +\infty$. In the outer region, v_e is exponentially small, and u_e is given in terms of the Green's function G of (5.7) by

$$u_e \sim 1 - \frac{G(\rho;\rho_0)}{G(\rho_0;\rho_0)} + O(\varepsilon)\,. \tag{5.14}$$

Next, we analyze zigzag instabilities of this ring solution. We introduce a perturbation in the form

$$v = v_e + e^{\lambda t} e^{im\theta}\phi\,, \qquad u = u_e + e^{\lambda t} e^{im\theta}\eta\,, \qquad . \tag{5.15}$$

where $\phi \ll 1$, $\eta \ll 1$, and m is a non-negative integer. Substituting (5.15) into (1.3), we obtain the following eigenvalue problem on $0 < \rho < R$ in place of (3.2):

$$\lambda\phi = \varepsilon^2\left(\phi_{\rho\rho} + \frac{1}{\rho}\phi_\rho\right) - \frac{\varepsilon^2 m^2}{\rho^2}\phi - \phi + 2Au_e v_e\phi + Av_e^2\eta\,, \tag{5.16 a}$$

$$\tau\lambda\eta = \eta_{\rho\rho} + \frac{1}{\rho}\eta_\rho - \frac{m^2}{\rho^2}\eta - \eta - 2u_e v_e\phi - v_e^2\eta\,. \tag{5.16 b}$$

This problem is studied in the inner region, where $\rho - \rho_0 = O(\varepsilon)$, and in the outer region where $\rho - \rho_0 = O(1)$.

In the inner region, we let $r = \varepsilon^{-1}(\rho - \rho_0)$ and from a dominant balance argument we write

$$u_e = \frac{\varepsilon}{A}U\,, \quad v_e = \frac{V}{\varepsilon}\,, \quad \phi = \frac{\Phi}{\varepsilon}\,, \quad \eta = \frac{\varepsilon N}{A}\,, \quad r = \varepsilon^{-1}(\rho - \rho_0)\,. \tag{5.17}$$

In terms of these variables, (5.16) reduces to an eigenvalue problem on $-\infty < r < \infty$

$$\lambda\Phi = \Phi'' + \frac{\varepsilon}{\rho_0 + \varepsilon r}\Phi' - \frac{\varepsilon^2 m^2}{(\rho_0 + \varepsilon r)^2}\Phi - \Phi + V^2 N + 2VU\Phi\,, \tag{5.18 a}$$

$$\tau\varepsilon^2\lambda N = N'' + \frac{\varepsilon}{\rho_0 + \varepsilon r}N' - \frac{\varepsilon^2 m^2}{(\rho_0 + \varepsilon r)^2}N - \varepsilon^2 N - V^2 N - 2VU\Phi\,. \tag{5.18 b}$$

We first assume that $m = O(1)$ as $\varepsilon \to 0$. By expanding V, U, Φ, and N, in powers of εA, and writing $\lambda = \varepsilon A\lambda_0$,

we derive (3.6) for Φ_0 and N_0. Thus, $\Phi_0 = V_0^{'}$ and $N_0 = U_0^{'}$. The system for Φ_1 and N_1 is (3.7), with the terms $-\Phi_0^{'}/(A\rho_0)$ and $-N_0^{'}/(A\rho_0)$ added to the right-hand side of (3.7). Since these additional terms are even functions, they do not contribute to the solvability condition that determines λ_0. Therefore, the entire analysis of (3.10)–(3.13) can be repeated, and we obtain that λ_0 satisfies (3.14).

To determine $N_1^{'}(\pm\infty)$ in (3.14) we must consider the outer region. By modifying the analysis of (3.18)–(3.19), we obtain the following outer problem for η on $0 < \rho < R$ in place of (3.20):

$$\eta_{\rho\rho} + \frac{1}{\rho}\eta_\rho - \frac{m^2}{\rho^2}\eta - (1+\tau\lambda)\eta = \frac{2B\varepsilon}{A}\delta^{'}(\rho-\rho_0) + \varepsilon\left[N_1^{'}(+\infty) - N_1^{'}(-\infty)\right]\delta(\rho-\rho_0)\,, \tag{5.19}$$

with $\eta_\rho(R) = 0$ and $\eta_\rho(0) = 0$. The matching condition of the inner and outer solutions for η is

$$\frac{\varepsilon}{A}\left(N_0 + \varepsilon A N_1 + \cdots\right) \sim \eta\left(\rho_0^{\pm}\right) + \varepsilon r\eta_\rho\left(\rho_0^{\pm}\right) + \cdots\,. \tag{5.20}$$

Since $N_0 = U_0^{'}$ satisfies $N_0(\pm\infty) = \pm B$, we get from this matching condition that

$$\eta\left(\rho_0^{\pm}\right) = \pm\frac{\varepsilon B}{A} = \pm\frac{\varepsilon}{2G(\rho_0;\rho_0)}\,, \qquad N_1^{'}(\pm\infty) = \varepsilon^{-1}\eta_\rho\left(\rho_0^{\pm}\right)\,. \tag{5.21}$$

Solving (5.19) for $\eta(\rho)$, we obtain

$$\eta(\rho) = \eta(\rho_0^{+})J_{2,m}(\rho)/J_{2,m}(\rho_0)\,, \quad \rho < \rho_0 < R\,; \qquad \eta(\rho) = \eta(\rho_0^{-})J_{1,m}(\rho)/J_{1,m}(\rho_0)\,, \quad 0 < \rho < \rho_0\,. \tag{5.22 a}$$

Here $J_{1,m}$ and $J_{2,m}$ are defined by

$$J_{2,m}(\rho) \equiv K_m(\theta\rho) - \frac{K_m^{'}(\theta R)}{I_m^{'}(\theta R)}I_m(\theta\rho)\,, \qquad J_{1,m}(\rho) \equiv I_m(\theta\rho)\,, \qquad \theta \equiv \sqrt{1+\tau\lambda}\,, \tag{5.22 b}$$

where I_m and K_m are modified Bessel's functions of order m. By using (5.21), (5.22), and the Wronskian relation $\mathcal{W}(J_{2,m}, J_{1,m}) = 1/\rho_0$ when $\rho = \rho_0$, we obtain the compact formula

$$N_1^{\prime}(+\infty) + N_1^{\prime}(-\infty) = -\left[2\rho_0^2 J_1(\rho_0)J_2(\rho_0)J_{1,m}(\rho_0)J_{2,m}(\rho_0)\right]^{-1}\,. \tag{5.23}$$

Substituting (5.23) into (3.14), and recalling that $\lambda \sim \varepsilon A\lambda_0$, we obtain the following main result for λ:

Principal Result 5.2: *Consider the equilibrium ring solution of Principal Result 5.1. Then, for a perturbation of the form (5.15) with $m = O(1)$ as $\varepsilon \to 0$, the zigzag eigenvalue λ satisfies the transcendental equation*

$$\lambda \sim -\varepsilon A\alpha\left(1 - \frac{1}{4\rho_0^2 J_1(\rho_0)J_2(\rho_0)J_{1,m}(\rho_0)J_{2,m}(\rho_0)}\right)\,. \tag{5.24}$$

Here $\alpha = \alpha(B)$, defined in (3.24), is positive along the primary branch of the $\gamma = \gamma(B)$ curve associated with the core problem of §2 (see Fig. 2). In (5.24), J_1 and J_2 are defined in (5.7) in terms of the domain radius R. In addition, $J_{1,m}$ and $J_{2,m}$, given in (5.22 b), depend on $\lambda\tau$. For $\tau = O(1)$, then $\tau\lambda \ll 1$. Therefore, $\theta \sim 1$ in (5.22 b). Setting $\theta = 1$ in (5.22 b), we conclude from (5.24) that there is a zigzag instability if and only if

$$4\rho_0^2 J_1(\rho_0)J_2(\rho_0)J_{1,m}(\rho_0)J_{2,m}(\rho_0) < 1\,. \tag{5.25}$$

We will only consider the case where $\tau = O(1)$ as $\varepsilon \to 0$. Since $\lambda = O(\varepsilon)$, we get $\theta = 1 + O(\varepsilon)$. Therefore, we set $\theta = 1$ in (5.22 b). In this case, the well-known asymptotic expansions of I_m and K_m for large m and fixed

R shows that $J_{1,m}J_{2,m} = O\left(m^{-1}\right)$ for $m \gg 1$ and ρ_0 fixed. Therefore, from (5.25), we have an instability if m is large enough. Although we cannot analytically determine the first unstable zigzag mode m_{zr} for arbitrary R, we can calculate m_{zr} for both $R \ll 1$ and $R \gg 1$. This leads to the next result.

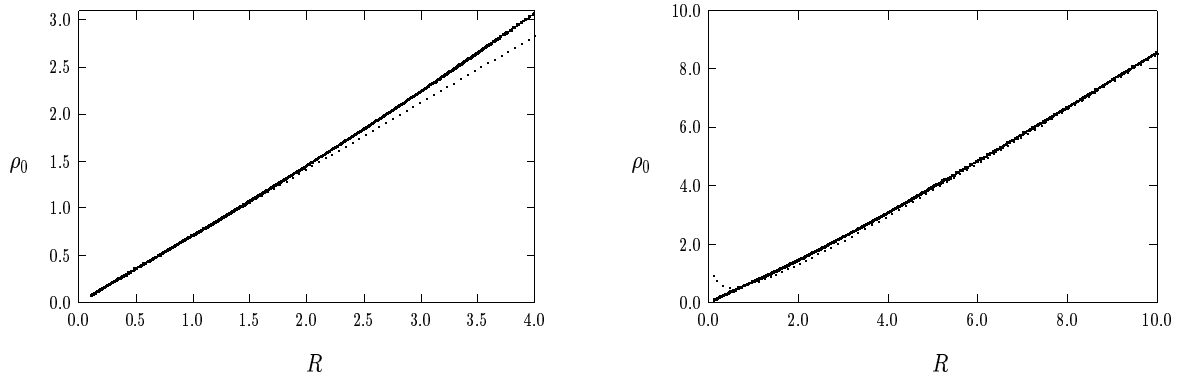

(a) ρ_0 versus R (small R)

(b) ρ_0 versus R (large R)

FIGURE 6. Comparison of numerically computed curves ρ_0 versus R (solid curves) with limiting result (5.26) for $R \ll 1$ (dotted curve, left figure), and the limiting result (5.26) for $R \to \infty$ (dotted curve, right figure).

Principal Result 5.3: *The following asymptotic formulae relate the domain radius R and the equilibrium ring radius ρ_0, as defined by the solution to (5.11):*

$$R \sim \sqrt{2}\rho_0\,, \quad \text{as} \quad R \to 0\,; \qquad R \sim \rho_0 + \frac{1}{2}\ln(2\rho_0) + O(\rho_0^{-1})\,, \quad \text{as} \quad R \to \infty\,. \tag{5.26}$$

Let m_{zr} be the smallest mode m for a zigzag instability when $\tau = O(1)$. Then,

$$m_{zr} = 3\,, \quad \text{as} \quad R \to 0\,; \qquad m_{zr} \sim \sqrt{2\rho_0} \sim \sqrt{2(R - \frac{1}{2}\ln(2R) + \cdots)}\,, \quad \text{as} \quad R \to \infty\,. \tag{5.27}$$

In Fig. 6 we compare the curve ρ_0 versus R computed numerically from (5.11) with the limiting results in (5.26) for $R \ll 1$ and for $R \gg 1$. These limiting results compare very favorably with the full numerical result. In Fig. 7 we plot the first unstable mode $m = m_{zr}$ versus $R = 1/\sqrt{D}$, obtained numerically from (5.25) and (5.11). This figure confirms that the first two modes $m = 1, 2$ are stable for any $R > 0$. Also note that m_{zr} increases as the domain radius R is increased. The asymptotic threshold $m_{zr} \sim \sqrt{2\rho_0}$ for $R \gg 1$ is shown in Fig. 7 to compare favorably with the numerical result for the threshold of (5.25) when $R \gg 1$. Numerical values for ρ_0 and m_{zr} are given in Table 2 together with the limiting approximations of Principal Result 5.3.

Firstly, we derive (5.26) and (5.27) for ρ_0 and m_{zr} when $R \to 0$. Bu using (5.7), we can write (5.11) as

$$\frac{K_0(\rho_0)}{I_0(\rho_0)} - \frac{K_0'(R)}{I_0'(R)} = \frac{1}{2\rho_0 I_0(\rho_0) I_0'(\rho_0)}\,. \tag{5.28}$$

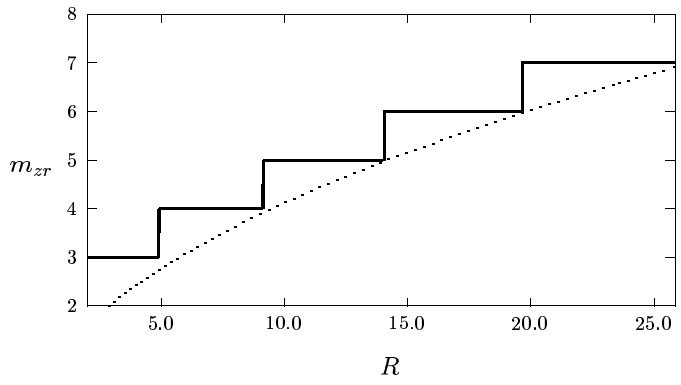

FIGURE 7. Plot of the first unstable zigzag mode m_{zr} versus the ring radius R for $\tau = O(1)$ computed from (5.25). The dotted line is the asymptotic curve (5.27) for $R \gg 1$.

D	R	ρ_0	ρ_0 $(R \ll 1)$	ρ_0 $(R \gg 1)$	m_{zr}	m_{zr} $(R \gg 1)$
5.0000	0.4472	0.3167	0.3162	0.5030	3	1.0030
3.0000	0.5774	0.4092	0.4082	0.5054	3	1.0054
1.0000	1.0000	0.7121	0.7071	0.6534	3	1.1432
0.7500	1.1547	0.8241	0.8165	0.7362	3	1.2134
0.5000	1.4142	1.0138	1.0000	0.8944	3	1.3374
0.2500	2.0001	1.4520	1.4143	1.3069	3	1.6167
0.1000	3.1626	2.3704	2.2363	2.2403	3	2.1167
0.0745	3.6644	2.7871	2.5911	2.6685	3	2.3102
0.0500	4.4730	3.4799	3.1629	3.3774	3	2.5990
0.0255	6.2634	5.0795	4.4289	4.9995	4	3.1621
0.0102	9.9093	8.4746	7.0069	8.4160	5	4.1027
0.0051	14.0280	12.4072	9.9193	12.3609	5	4.9721
0.0030	18.1343	16.3777	12.8229	16.3389	6	5.7164
0.0020	22.2473	20.3833	15.7312	20.3497	7	6.3796
0.0010	31.6228	29.5754	22.3607	29.5493	8	7.6876

Table 2. Numerical values for ρ_0 for various values of $R = 1/\sqrt{D}$ computed from (5.28). The fourth and fifth columns are the asymptotic approximations in (5.26). The sixth column is the first (integer) unstable zigzag mode m_{zr} from (5.25). The last column is m_{zr} for $R \gg 1$ from (5.27).

For $R \to 0$, with $0 < \rho_0 < R$, we use the small argument expansions of I_0 and K_0 to obtain that

$$2\rho_0 I_0(\rho_0) I_0'(\rho_0) \sim \rho_0^2\,, \qquad \frac{K_0'(R)}{I_0'(R)} \sim -2R^{-2}\,, \qquad \frac{K_0(\rho_0)}{I_0(\rho_0)} \sim -\ln\rho_0\,.$$

Therefore, (5.28) reduces to $2R^{-2} \sim \rho_0^{-2}$. This yields $R \sim \sqrt{2}\rho_0$, which establishes (5.26) for $R \to 0$.

Next, we calculate m_{zr} for $R \to 0$. By using the local behavior of $I_0(z)$ and $K_0(z)$ for $z \ll 1$, we get

$$J_1(\rho_0) J_2(\rho_0) \sim \frac{2}{R^2} \sim \rho_0^{-2}\,. \tag{5.29}$$

Substituting the small argument expansions

$$K_m(\rho_0) \sim \frac{1}{2}\Gamma(m)\left(\frac{\rho_0}{2}\right)^{-m} \qquad I_m(\rho_0) \sim \frac{1}{\Gamma(m+1)}\left(\frac{\rho_0}{2}\right)^{m} \tag{5.30}$$

and $\theta = 1$ into (5.22 *b*), where $\Gamma(m)$ is the Gamma function, we obtain for $R \ll 1$ and $\rho \ll 1$ that

$$J_{1,m}(\rho_0)J_{2,m}(\rho_0) = I_m(\rho_0)K_m(\rho_0) - \frac{K_m'(R)}{I_m'(R)}\left(I_m(\rho_0)\right)^2 \sim \frac{1}{2}\frac{\Gamma(m)}{\Gamma(m+1)}\left(1+\frac{1}{2^m}\right). \tag{5.31}$$

Therefore, substituting (5.29) and (5.31) into (5.25), we have instability when $R \ll 1$ if and only if

$$\frac{m}{1+2^{-m}} - 2 > 0\,. \tag{5.32}$$

The first integer for which (5.32) holds is $m_{zr} = 3$, which establishes (5.27) for $R \to 0$.

Secondly, we derive the results in Principal Result 5.3 for $R \gg 1$. To do so, we need the asymptotic formulae

$$K_0(z) \sim \sqrt{\frac{\pi}{2z}}e^{-z}\left(1-\frac{1}{8z}\right), \qquad I_0(z) \sim \sqrt{\frac{1}{2\pi z}}e^{z}\left(1+\frac{1}{8z}\right), \qquad z \gg 1\,. \tag{5.33}$$

By using these formulae of [**2**], we readily derive

$$\frac{K_0(\rho_0)}{I_0(\rho_0)} \sim \frac{\pi}{e^{2\rho_0}}\left(1-\frac{1}{4\rho_0}\right), \quad \frac{K_0'(R)}{I_0'(R)} \sim -\frac{\pi}{e^{2R}}\left(1-\frac{3}{4R}\right), \quad I_0(\rho_0)I_0'(\rho_0) \sim \frac{e^{2\rho_0}}{2\pi\rho_0}\left(1-\frac{1}{4\rho_0}\right).$$

Substituting these expressions into (5.28), we obtain that

$$\frac{e^{-2\rho_0}}{2\rho_0} \sim e^{-2R}\left(1-\frac{3}{4R}\right). \tag{5.34}$$

For $R \gg 1$, the asymptotic solution to (5.34) is $R \sim \rho_0 + \frac{1}{2}\ln(2\rho_0)$. This establishes (5.26) for $R \gg 1$.

Finally, we establish the stability threshold (5.27) for m_{zr} when $R \gg 1$. By using (5.33) and (5.26), we obtain

$$J_1(\rho_0)J_2(\rho_0) \sim \frac{1}{2}\left(1+e^{2\rho_0-2R}\right) \sim \frac{1}{2\rho_0}\left(1+\frac{1}{2\rho_0}\right). \tag{5.35}$$

Next, we must estimate $J_{1,m}(\rho_0)J_{2,m}(\rho_0)$. Since, we have $m_{zr} \gg 1$ and $\rho_0 \gg 1$, we must use the following *uniform* expansions of $K_m(mz)$ and $I_m(mz)$ for $m \to \infty$ as given in [**2**]:

$$K_m(mz) \sim \sqrt{\frac{\pi}{2m}}\frac{e^{-m\beta(z)}}{(1+z^2)^{1/4}}, \quad I_m(mz) \sim \frac{1}{\sqrt{2\pi m}}\frac{e^{m\beta(z)}}{(1+z^2)^{1/4}}, \quad \beta(z) \equiv \sqrt{1+z^2} + \ln\left(\frac{z}{1+\sqrt{1+z^2}}\right). \tag{5.36}$$

Defining z and z_1 by $z \equiv \rho_0/m$ and $z_1 \equiv R/m$, we obtain from (5.36) that

$$J_{1,m}(\rho_0)J_{2,m}(\rho_0) \sim \frac{1}{2m\sqrt{1+z^2}}\left(1+e^{2m[\beta(z)-\beta(z_1)]}\right). \tag{5.37}$$

Since $R \sim \rho_0 + \frac{1}{2}\ln(2\rho_0)$, we have that $z - z_1 \to 0$ provided that $\ln(\rho_0)/m \ll 1$. Assuming for the moment that this condition is true, we can then use $\beta'(z) = z^{-1}\sqrt{1+z^2}$ to estimate

$$\beta(z) - \beta(z_1) \sim \beta'(z)(z-z_1) \sim -\frac{\ln(2\rho_0)}{2mz}\sqrt{1+z^2}\,.$$

Substituting this expression into (5.37), and using (5.35), the stability threshold condition of (5.25) becomes

$$\frac{z}{\sqrt{1+z^2}}\left(1+\frac{1}{2\rho_0}\right)\left(1+e^{-\ln(2\rho_0)z^{-1}\sqrt{1+z^2}}\right) \sim 1\,, \tag{5.38}$$

where $z \equiv \rho_0/m$. If we assume that $z = O(1)$ and $\rho \gg 1$, then it is easy to see that there is no root to (5.38). Therefore, we must assume that $z \gg 1$. In this limit, (5.38) reduces to

$$\frac{z}{\sqrt{1+z^2}}\left(1+\frac{1}{2\rho_0}\right)^2 \sim 1\,.$$

It readily follows that that $\rho_0 \sim 2z^2$. Since $z = \rho_0/m$, we get $m \sim \sqrt{2\rho_0}$, which establishes (5.27) for $R \gg 1$. The consistency condition $\ln(2\rho_0)/m \ll 1$ needed above is indeed satisfied.

Next, we consider how the zigzag instability of the ring for modes with $m > m_{zr}$ is re-stabilized for asymptotically large modes where $m \to \infty$ as $\varepsilon \to 0$. Similar to our study in §3 of zigzag instabilities of the stripe solution, we find that the ring re-stabilizes when $m = O(\varepsilon^{-1})$. In this regime, we introduce m_0 by $m = m_0\varepsilon^{-1}$, where $m_0 = O(1)$. From (5.18), we obtain the following leading-order eigenvalue problem defined on $-\infty < r < \infty$:

$$\left(\lambda + \frac{m_0^2}{\rho_0^2}\right)\Phi_0 = \Phi_0'' - (1-2V_0U_0)\,\Phi_0 + V_0^2 N_0\,, \qquad \frac{m_0^2}{\rho_0^2}N_0 = N_0'' - V_0^2 N_0 - 2V_0U_0\Phi_0\,. \tag{5.39}$$

We seek an odd eigenfunction to (5.39) with $\Phi_0 \to 0$ and $N_0 \to 0$ as $r \to \pm\infty$. This problem is precisely the stripe eigenvalue problem (3.32) once we replace m_0 in (3.32) with m_0/ρ_0. This leads to the next main result.

Principal Result 5.4: *Consider the equilibrium ring solution of Principal Result 5.1. Then, all zigzag perturbations of the form (5.15) are unstable in the zone $m_{zr} < m < \varepsilon^{-1}\rho_0 m_{0z}$, and are stable outside of this zone. Here m_{zr} is the root of*

$$4\rho_0^2 J_1(\rho_0)J_2(\rho_0)J_{1,m}(\rho_0)J_{2,m}(\rho_0) = 1\,, \tag{5.40}$$

which depends on R. The threshold m_{0z}, computed in §3 and plotted in Fig. 4(a), depends on the value of B associated with the core problem. Here $B = A/[2\rho_0 J_1(\rho_0)J_2(\rho_0)]$, where ρ_0 is determined in terms of R by (5.11). In the intermediate regime, $O(\varepsilon^{1/2}) \ll A \ll O(1)$, the zigzag instability band is

$$m_{zr} < m < \frac{A^2}{6\varepsilon\rho_0 J_1^2(\rho_0)J_2^2(\rho_0)}\,. \tag{5.41}$$

In Fig. 8(a) we plot B/A as a function of the domain radius R. A simple calculation using (5.7), (5.26), and (5.33), shows that $B \sim A\,[1+1/(2R)]^{-1}$ for $R \gg 1$. Recall that there is no equilibrium solution if $B > 1.347$. Our final result gives the stability properties of a ring with respect to breakup instabilities.

Principal Result 5.5: *Consider the equilibrium ring solution given in Principal Result 5.1 in the intermediate $O(\varepsilon^{1/2}) \ll A \ll O(1)$. Such a solution is unstable with respect to perturbations of the form (5.15), where ϕ and η are now even functions in the inner region, if and only if*

$$\frac{A^2}{12\rho_0 J_1^2(\rho_0)J_2^2(\rho_0)} < \varepsilon m < \frac{\sqrt{5}}{2}\rho_0\,, \tag{5.42}$$

where J_1 and J_2 are defined in (5.7). In the high feed-rate regime, the instability band is

$$\sqrt{\mu_1}\rho_0 < \varepsilon m < \sqrt{\mu_2}\rho_0\,, \tag{5.43}$$

where $\mu_1 = \mu_1(B)$ and $\mu_2 = \mu_2(B)$ are given in Table 1 and plotted in Fig. 5. Here ρ_0 is determined in terms of R by (5.11), and $B = A/[2\rho_0 J_1(\rho_0)J_2(\rho_0)]$.

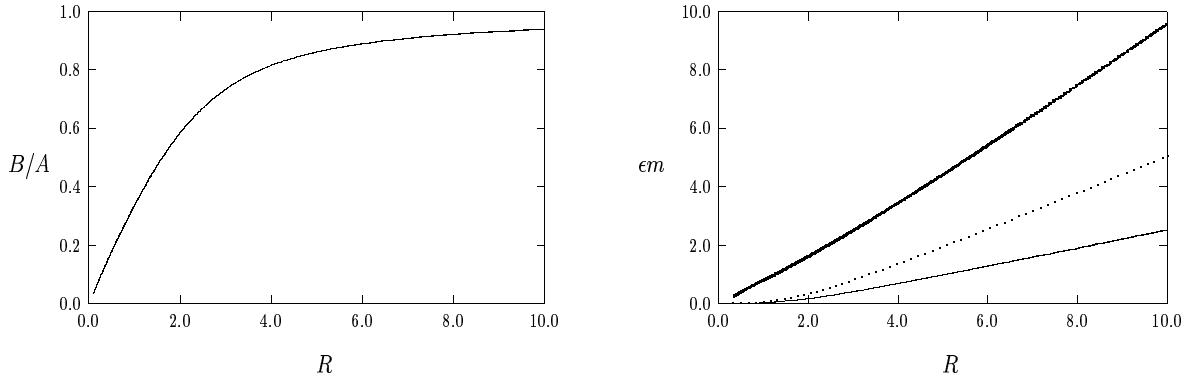

(a) B/A versus R (b) εm versus R

FIGURE 8. Left figure: plot of B/A versus the domain radius R. Right figure: the breakup instability bounds in (5.42) for εm in the intermediate regime versus R. The lower bound (solid curve) is for $A = 1$. The upper bound is the heavy solid curve. The dotted curve is the upper bound for the zigzag instability band in the intermediate regime when $A = 1$.

In Fig. 8(b) we plot the upper and lower bounds in (5.42), which determine the breakup instability bounds for εm in the intermediate regime, as a function of R. The lower bound in (5.42) is plotted for $A = 1$.

The result (5.43) follows immediately by noting that the eigenvalues problems (4.2) and (5.39) for the stripe and ring, respectively, are equivalent if we replace $\mu = \varepsilon^2 m^2$ in (4.2) with $\mu = \varepsilon^2 m^2/\rho_0^2$. The result (5.42) is also readily obtained from modifying the analysis in §4. To obtain (5.42), we repeat the analysis of (4.3)–(4.14). The upper bound in (5.42) follows from (4.4). Then, to determine the lower bound in (5.42), we re-derive the nonlocal eigenvalue problem (4.14), where the multiplier χ in (4.14) is to be replaced with

$$\chi = 2\left[1 + \frac{\varepsilon\delta^{-2}}{6G_m(\rho_0;\rho_0)}\right]^{-1}, \qquad G_m(\rho_0;\rho_0) \equiv \rho_0 J_{1,m}(\rho_0) J_{2,m}(\rho_0)\,. \tag{5.44}$$

Here $G_m(\rho_0;\rho_0)$ is the Green's function, evaluated at $\rho = \rho_0$, for $\eta'' + \rho^{-1}\eta' - m^2\rho^{-2}\eta = -\delta(\rho - \rho_0)$ with $\eta'(0) = \eta'(R) = 0$. In (5.44), $J_{1,m}$ and $J_{2,m}$ are defined in (5.22 *b*). From Lemma 4.1, the stability threshold is at $\chi = 1$. Since $\varepsilon\delta^{-2} \ll 1$ in the intermediate regime where $\delta \gg O(\varepsilon^{1/2})$, we conclude that all modes with $m = O(1)$ are stable. However, since $J_{1,m}J_{2,m} \sim (2m)^{-1}$ as $m \to \infty$ for fixed ρ_0, then $\chi < 1$ when $m < 3\delta^2\rho_0/\varepsilon$. Finally, since $\delta \sim B/3$, and B is related to A by $B = A/[2G(\rho_0;\rho_0)]$, we obtain the lower bound in (5.42).

6 Qualitative Discussion and the Weak Interaction Regime

In Table 3 we summarize our results of §3–§5 for breakup and zigzag instability bands for a ring and a stripe in both the low and high feed-rate regimes. We now qualitatively discuss the implications of these results and their dependence on the parameters. We also comment on the stability of a stripe for the Gierer-Meinhardt model.

For a stripe, the upper bounds for both the zigzag and the breakup instabilities determine critical domain

Geometry	Regime	Breakup Instability Band	Zigzag Instability Band
Ring	HF: $A = O(1)$	$\frac{\rho_0\sqrt{\mu_1}}{\varepsilon} < m < \frac{\rho_0\sqrt{\mu_2}}{\varepsilon}$	$m_{zr} < m < \frac{\rho_0 m_{0z}}{\varepsilon}$
Ring	INT: $O(\varepsilon^{1/2}) \ll A \ll O(1)$	$\frac{A^2}{12\varepsilon\rho_0 J_1^2(\rho_0)J_2^2(\rho_0)} < m < \frac{\sqrt{5}\rho_0}{2\varepsilon}$	$m_{zr} < m < \frac{A^2}{6\varepsilon\rho_0 J_1^2(\rho_0)J_2^2(\rho_0)}$
Stripe	HF: $A = O(1)$	$\frac{\sqrt{\mu_1}}{\varepsilon} < \frac{k\pi}{d} < \frac{\sqrt{\mu_2}}{\varepsilon}$	$m_{zs} < \frac{k\pi}{d} < \frac{m_{0z}}{\varepsilon}$
Stripe	INT: $O(\varepsilon^{1/2}) \ll A \ll O(1)$	$\frac{A^2\tanh^2 l}{3\varepsilon} < \frac{k\pi}{d} < \frac{\sqrt{5}}{2\varepsilon}$	$m_{zs} < \frac{k\pi}{d} < \frac{2A^2\tanh^2 l}{3\varepsilon}$

Table 3. Breakup and zigzag instability bands for the ring, with angular integer mode m, and the stripe, with integer mode k, in the high feed-rate and intermediate regimes. Here m_{zs} is the root of (3.25), depending on $l = 1/\sqrt{D}$, plotted in Fig. 3, and m_{zr} is the root of (5.40), depending on $R = 1/\sqrt{D}$, plotted in Fig. 7 and given in Table 2. The thresholds m_{0z}, μ_1, and μ_2, plotted in Fig. 5(a) and given in Table 1 depend on the parameter B associated with the core problem. For the stripe $B = A\tanh l$, and for the ring $B = A/[2\rho_0 J_1(\rho_0)J_2(\rho_0)]$. The ratio B/A and the ring radius ρ_0 are plotted versus the domain radius R in Fig. 8(a) and Fig. 6, respectively.

widths for stability with respect to all integers k. In particular, consider zigzag instabilities in the high feed-rate regime. Table 3 shows that an equilibrium stripe solution for (1.3) is stable with respect to all zigzag modes when $\pi/d > m_{0z}/\varepsilon$. Since $\varepsilon = \varepsilon_0 l$ and $d = l d_0$ from (1.3 d) and (1.3 c), it follows that an equilibrium stripe solution for the GS model (1.1) is stable with respect to all zigzag modes when the domain width d_0 satisfies

$$d_0 < d_{0sz}^{\rm h} \equiv \frac{\pi\varepsilon_0}{m_{0z}}\,, \qquad A = O(1)\,. \tag{6.1}$$

Therefore, the critical domain width in (1.1) for stability is $O(\varepsilon_0) \ll 1$. In a similar way, we use Table 3 to show that an equilibrium stripe solution for the original GS model (1.1) in the high feed-rate regime is stable with respect to all breakup modes when the domain width d_0 satisfies

$$d_0 < d_{0sb}^{\rm h} \equiv \frac{\pi\varepsilon_0}{\sqrt{\mu_2}}\,, \qquad A = O(1)\,. \tag{6.2}$$

In (6.1) and (6.2), the critical values m_{0z} and $\sqrt{\mu_2}$ are plotted in Fig. 5(a) versus $B = A\tanh l$, and they are tabulated in Table 1. From Fig. 5(a) it is clear that the zigzag and breakup instability bands overlap in the high feed-rate regime. However, since $\sqrt{\mu_2} > m_{0z}$ as shown in Table 1 and Fig. 5(a), it follows that $d_{0sb}^{\rm h} < d_{0sz}^{\rm h}$. Therefore, in the high feed-rate regime, there is no domain width d_0 where a zigzag instability is not accompanied by a breakup instability. However, for d_0 in $d_{0sb}^{\rm h} < d_0 < d_{0sz}^{\rm h}$, then only breakup instabilities can occur. Comparing Fig. 5(b) with Fig. 4(b), where we plot the growth rates, we find that the time-scales of breakup and zigzag instabilities in the high feed-rate regime are both $O(1)$ for modes $m = O(\varepsilon^{-1})$.

For a stripe in the intermediate regime $O(\varepsilon^{1/2}) \ll A \ll O(1)$, we can also use Table 3 to determine critical domain widths $d_{0sz}^{\rm i}$ and $d_{0sb}^{\rm i}$ for zigzag and breakup instabilities, respectively, as

$$d_{0sz}^{\rm i} \equiv \frac{3\pi\varepsilon_0}{2A^2\tanh^2 l}\,, \qquad d_{0sb}^{\rm i} \equiv \frac{2\pi\varepsilon_0}{\sqrt{5}}\,, \qquad O(\varepsilon_0^{1/2}) \ll A \ll O(1)\,. \tag{6.3}$$

Since the lower threshold of the breakup instability band is smaller than for the high feed-rate regime, a stripe can break up into fewer spots in the intermediate regime. Another observation is that in contrast to the rather

narrow range of domain widths d_0 for the high feed-rate regime, there is now a larger range of values of d_0, now satisfying $d_{0sb}^{\rm i} < d_0 < d_{0sz}^{\rm i}$, where a breakup instability can occur with no zigzag instability. Since $d_{0sz}^{\rm i} > d_{0sz}^{\rm h}$, the zigzag instabilities of a stripe are more prevalent in the high feed-rate regime in the sense that they can only be prevented by taking a much smaller domain width than in the intermediate regime. From (3.41) the growth rate λ_0 of zigzag perturbations near the upper stability threshold in the intermediate regime is $O(A^4) \ll 1$. Therefore, a zigzag instability in this regime develops more slowly than in the high feed-rate regime.

Another observation is that for a stripe in the intermediate regime, the zigzag instability band in Table 3 can disappear if the domain length $l = 1/\sqrt{D}$ is sufficiently small, or equivalently if the diffusivity D of u in (1.1) is large enough. For $l \ll 1$, we have from (3.25) that $m_{zs} \sim \omega/l$, where $\omega = 1.1997$ is the root of $\omega \tanh \omega = 1$. Therefore, from Table 3, the zigzag instability band is

$$\frac{\omega}{l} < \frac{k\pi}{d} < \frac{2A^2 l^2}{3\varepsilon}\,. \tag{6.4}$$

Since $\varepsilon = \varepsilon_0 l$ from (1.3 *d*), the two bounds in (6.4) coincide when $\omega/l = 2A^2 l/(3\varepsilon_0)$. Solving for $D = l^{-2}$, we conclude that there are no zigzag instabilities in the near-shadow limit $D \gg 1$, when $D > D_c$, where

$$D_c \equiv \frac{2A^2}{3\omega\varepsilon_0} = 0.555\left(\frac{A^2}{\varepsilon_0}\right)\,. \tag{6.5}$$

For completeness, we now give a result for zigzag and breakup instabilities of a stripe for the GS model (1.3) in the low feed-rate regime $A = O(\varepsilon^{1/2})$. The result, with the derivation outlined in Appendix A, is as follows:

Principal Result 6.1: *Let $\varepsilon \to 0$, $A = \varepsilon^{1/2}\mathcal{A}$ with $\mathcal{A} = O(1)$. Then, when $\mathcal{A} > \mathcal{A}_{1e} \equiv \sqrt{12\coth l}$, there are two equilibrium stripe solution branches, given in (A.2), that meet at the saddle-node value $\mathcal{A}_{1e}$. The equilibrium solution for v on the branch that merges onto the intermediate regime solution is parameterized in terms of s as*

$$v \sim \varepsilon^{-1/2}\frac{(s+1)}{\mathcal{A}} w\left(\varepsilon^{-1}x_1\right)\,, \qquad \mathcal{A} = \mathcal{A}_{1e}\frac{(1+s)}{2\sqrt{s}}\,, \qquad s \geq 1\,. \tag{6.6}$$

Here $w(y)$ is the homoclinic solution of (2.19). For τ below an $O(1)$ Hopf bifurcation threshold, the breakup instability band for this stripe solution is

$$m_{gsl} < \frac{k\pi}{d} < \frac{\sqrt{5}}{2\varepsilon}\,, \qquad m \equiv \frac{k\pi}{d}\,. \tag{6.7 a}$$

Here m_{gsl}, which depends on s and l, is the unique root $m = m_{gsl}$ of

$$\theta\tanh\left(l\theta\right) = s\tanh l\,, \qquad \theta \equiv \sqrt{1+m^2}\,. \tag{6.7 b}$$

Alternatively, zigzag instabilities are determined by zero-crossings of the small eigenvalue $\lambda = O(\varepsilon^2)$ given by

$$\lambda \sim \varepsilon^2\left(2s\left[\theta\tanh l\tanh(l\theta) - 1\right] - m^2\right)\,, \qquad \theta \equiv \sqrt{1+m^2}\,. \tag{6.8}$$

By comparing the breakup instability zone (6.7 *a*) with the GS intermediate regime result in Table 3, we observe that the critical domain width is the same, but that the lower bound $m_{gsl} = O(1)$ is asymptotically smaller than in the intermediate regime. Therefore, a breakup instability in the low feed-rate regime can lead to a fewer number of spots than in the intermediate or high feed-rate regimes. As a remark, we can recover the lower

bound in Table 3 for the intermediate regime $O(\varepsilon^{1/2}) \ll A \ll O(1)$, or equivalently $O(1) \ll \mathcal{A} \ll O(\varepsilon^{-1/2})$, by letting $s \to \infty$ in (6.7 b). For $s \gg 1$, we solve (6.7 b) to get $m_{gsl} \sim s \tanh l$. Then, using $s \sim 4\mathcal{A}^2/\mathcal{A}_{1e}^2 = \frac{1}{3}\mathcal{A}^2 \tanh l$ from (6.6), together with $\mathcal{A} = A\varepsilon^{-1/2}$, we get $m_{gsl} \sim \frac{A^2}{3\varepsilon} \tanh^2 l$. This agrees with the lower bound in the GS intermediate regime result in Table 3.

Regarding zigzag instabilities for the GS model in the low feed-rate regime, we set $\lambda = 0$ in (6.8) to get

$$\tanh(\theta l) \tanh l = \frac{1}{2s}\left[\theta + \frac{(2s-1)}{\theta}\right], \qquad \theta \equiv \sqrt{1+m^2}\,. \tag{6.9}$$

A simple graphical analysis shows that (6.9) has no roots for $1 < s < s_c$ and two roots when $s > s_c$, where s_c depends on l. Therefore, a zigzag instability zone $m_{zl} < m < m_{zu}$ exists only when the ratio $\mathcal{A}/\mathcal{A}_{1e}$ is sufficiently large. As a remark, we can readily recover the GS zigzag instability zone in Table 3 of the intermediate regime by taking the limit $s \to \infty$ in (6.9) where $s \sim \frac{1}{3}\mathcal{A}^2 \tanh l$. In this limit, the large root of (6.9) is $m_{zu} \sim 2s \tanh l \sim \frac{2}{3\varepsilon}A^2 \tanh l \gg 1$, while the smaller root m_{zl} tends to the root m_{zs} of (3.25).

The results in (6.7) and (6.8) for the low feed-rate GS model are similar to those for the stability of a stripe for the classical Gierer Meinhardt (GM) model of [**9**]. For the infinite strip $\mathbb{R}^1 \times [0,d]$ this problem was first studied in [**7**] with respect to breakup instabilities. Here we will summarize some results of [**19**] for zigzag and breakup instabilities of a stripe centered along the mid-line of the finite rectangular domain $\Omega = [-l,l] \times [0, ld_0]$ of (1.3 c). In order to readily compare results between the GM and GS models, we write the GM model as

$$a_t = \varepsilon^2 \Delta a - a + a^2/h\,, \quad \tau h_t = \Delta h - h + a^2/\varepsilon\,, \quad x = (x_1,x_2) \in \Omega\,, \ \ t > 0\,; \quad \partial_n a = \partial_n h = 0\,, \quad x \in \partial\Omega\,. \tag{6.10}$$

In the semi-strong regime $l = O(1)$ and $\varepsilon \ll 1$, a matched asymptotic analysis gives the equilibrium solution

$$a_e(x_1) = \mathcal{H} w\left[\varepsilon^{-1}x_1\right], \qquad h_e(x_1) \equiv \mathcal{H}\frac{G_l(x_1)}{G_l(0)}, \qquad \mathcal{H} = \frac{1}{3}\tanh l\,. \tag{6.11}$$

Here $w(y)$ and $G_l(x_1)$ satisfy (2.19) and (2.7), respectively. We then introduce a perturbation in the form

$$a = a_e(x_1) + e^{\lambda t + imx_2}\phi(x_1)\,, \qquad h = h_e(x_1) + e^{\lambda t + imx_2}\eta(x_1)\,. \tag{6.12}$$

For $\tau \ll O(\varepsilon^{-2})$, it is shown in Principal Result 2.4 of [**19**] that the growth rate λ of a zigzag mode m is

$$\lambda \sim \varepsilon^2\left[2\theta \tanh(\theta l)\tanh l - (m^2+2)\right], \qquad \theta \equiv \sqrt{1+m^2}\,. \tag{6.13}$$

Setting $\lambda = 0$ to get the instability threshold, we obtain

$$\tanh(\theta l)\tanh l = h(\theta) \equiv \frac{\theta^2+1}{2\theta}, \qquad \theta = \sqrt{m^2+1}\,. \tag{6.14}$$

Since the minimum of $h(\theta)$ is $h(1) = 1$, it follows that (6.14) has no roots for any $\theta \geq 0$. Therefore, in contrast to the GS model, there are no zigzag instabilities for the classical GM model in the semi-strong regime.

For τ below an $O(1)$ Hopf bifurcation threshold, it was shown in Proposition 2.3 of [**19**] that the breakup instability band satisfies

$$m_{gm} < m < \frac{\sqrt{5}}{2\varepsilon}\,. \tag{6.15}$$

Here m_{gm}, which depends on the domain half-length l, is the unique root of

$$\theta \tanh(l\theta) = 2\tanh l\,, \qquad \theta \equiv \sqrt{1+m^2}\,. \tag{6.16}$$

Clearly $m_{gm} \sim 1$ for $l \to 0$, and $m_{gm} \sim \sqrt{3}$ for $l \to \infty$. For $l \gg 1$, the breakup instability band $\sqrt{3} < m < \frac{\sqrt{5}}{2\varepsilon}$, corresponding to a stripe on an infinite strip, was first given in a different form in Theorem 4.5 of [**7**].

The result (6.16) is similar to the breakup instability band (6.7) for a stripe solution to the GS model in the low feed-rate regime. Notice, however, that the corresponding lower bound for the GS model in the intermediate and high feed-rate regimes in Table 3 is asymptotically larger than in (6.15). This suggests that a stripe for the GS model in the high feed-rate regime can disintegrate into many more spots than in the low or intermediate feed-rate regimes, or for the GM model.

The main difference between a stripe and ring, is that the instability zones for the ring are determined in terms of the ring radius ρ_0, which depends on $R = 1/\sqrt{D}$. The results in Table 2 and (5.26) show that the equilibrium ring divides the circle of radius R into two equal areas when $D \gg 1$. For $D \ll 1$, (5.26) shows that the ring concentrates near the rim of the circle. Since the gradient of the outer solution for u away from the ring becomes smaller as D is decreased, the equilibrium ring must concentrate closer to the boundary when D is small in order to balance the curvature of the ring with the interaction of the outer solution for u and the boundary. The instability thresholds μ_1, μ_2, and m_{0z}, in Table 3, calculated for the stripe solution in Fig. 5(a) and Table 1 in terms of the core solution parameter B, also apply to the ring if we identify $B = A/[2\rho_0 J_1(\rho_0)J_2(\rho_0)]$. In contrast to the stripe where the lower zigzag bound m_{zs} satisfies $m_{zs} \to 0$ as $D \to 0$ (see Fig. 3), the lower zigzag bound m_{zr} for the ring satisfies $m_{zr} = \sqrt{2}D^{-1/4} \gg 1$ for $D \ll 1$. This difference in the behavior of the lower threshold results from the concentration of the equilibrium ring near the rim of the disk when D is small. In Appendix B we comment on some previous results in [**28**] for breakup instabilities of a ring when $A \ll O(1)$.

Self-replication behavior for the GS model in the semi-strong interaction regime occurs when $B > 1.347$. For the stripe, this implies that stripe-replication should occur when $A > 1.347\coth(D^{-1/2})$. For the one-dimensional problem in the semi-strong regime, where the stripe is replaced by a pulse, pulse-splitting behavior has been studied in [**38**], [**39**], [**5**], [**29**], and [**17**]. For the weak interaction regime, one-dimensional pulses for the GS model exhibit an edge-splitting process (cf. [**8**], [**33**], [**42**]). In §7 we show a stripe-replication process in the semi-strong regime where the replicating stripes undergo a breakup instability. For the related GM model (6.10) pulse-splitting behavior only occurs in the weak interaction regime where $l \gg 1$ with $\varepsilon = O(1)$, and it is of edge-splitting type (cf. [**7**], [**20**]). Self-replicating stripe solutions for the GM model in this weak interaction regime have been studied in [**7**]. For a ring solution to the GS model in the semi-strong regime, it was shown in [**22**] that the threshold $B = 1.347$ leads to the occurrence of self-replicating rings when $A > (2.694)\rho_0 J_1(\rho_0)J_2(\rho_0)$, where ρ_0 is the equilibrium ring radius. This behavior was shown in Fig. 10–12 of [**22**]. Ring-splitting behavior in this regime was also observed numerically in Fig. 12 of [**28**].

The result (6.15) for the GM model and the results in Table 3 for a stripe solution to the GS model all show that the upper bound of the breakup instability zone is $m = O(\varepsilon^{-1})$ for $\varepsilon \ll 1$. Therefore, a stripe can be stabilized with respect to breakup instabilities in the semi-strong regime only when the domain width d_0 is

$O(\varepsilon)$ thin. The final question that we discuss is whether it is possible to stabilize a stripe or a ring with respect to breakup instabilities by suitably changing the *intrinsic* parameters A and D. In the semi-strong interaction regime this is not possible, as we claim that each breakup instability band in Table 3 for the stripe and ring is never the empty set. In the high feed-rate regime, this follows from the inequality $\mu_1 < \mu_2$. In the intermediate regime, we use the relationship between A and B for the stripe and the ring to show that the breakup instability zone in Table 3 would disappear when $B^2/3 = \sqrt{5}/2$, which yields $B = 1.83$. However, this is inconsistent since $B < 1.347$ is needed for the existence of the core solution and $O(\varepsilon^{1/2}) \ll B \ll 1$ was the region of validity of the intermediate regime. Therefore, in the semi-strong interaction regime, the stripe can never be intrinsically stabilized with respect to breakup instabilities by varying A or D.

However, in the weak interaction regime, we now show numerically that a stripe can be stable with respect to breakup instabilities, but is unstable to zigzag instabilities. In (1.1) we write $y = x_1/\varepsilon_0$ and $D = D_0\varepsilon_0^2$ for some $D_0 = O(1)$. The resulting equilibrium problem is to look for even solutions to

$$v_{yy} - v + Auv^2 = 0\,, \quad D_0 u_{yy} - (u-1) - uv^2 = 0 \quad -\infty < y < \infty\,; \qquad v \to 0\,, \quad u \to 1\,, \quad |y| \to \infty\,. \tag{6.17}$$

To motivate our choice of parameter values in (6.17), we consider the following GS model studied numerically in [**37**] in a two-dimensional square domain:

$$V_T = D_V \triangle V - (F+k)V + UV^2 = 0\,, \qquad U_T = D_U \triangle U - F(U-1) - UV^2\,. \tag{6.18}$$

For the fixed ratio $D_U/D_V = 2$, and for various ranges of F and k, numerical results for (6.18) are given in [**37**] and are shown on the interactive website XMORPHIA [**49**]. In terms of our notation in (6.17), we calculate $A = \sqrt{F}/(F+k)$ and $D_0 \equiv D/\varepsilon_0^2 = 2(F+k)/F$. In [**37**] stable stripes where observed for $(k, F) = (0.06, 0.045)$, which yields $(A, D_0) = (2.02, 4.667)$. To interpret this result in terms of stability bands, we compute a solution branch of (6.17) that begins at a point in the semi-strong regime, taken to be $(A, D_0) = (1.5, 0.1L^2)$, for some $L \gg 1$, and that terminates at the point $(A, D_0) = (2, 4)$. The specific path, parameterized by p, is taken to be

$$D_0 = L^{2-p}\,, \qquad A = 2.0 - 0.5\left[\frac{(D_{0min}/D_0)^\sigma - 1}{(D_{0min}/D_{0max})^\sigma - 1}\right]\,, \qquad -\frac{\ln(0.1)}{\ln L} \equiv p_{min} \le p \le p_{max} = 2 - \frac{\ln 4}{\ln L}\,. \tag{6.19}$$

We choose $\sigma = 0.8$, $D_{0max} = 0.1L^2$, and $D_{0min} = 4.0$. At each point on this path we solve (6.17) numerically on the long domain $[0, L]$ with $v_y(L) = u_y(L) = 0$, and with the symmetry condition $v_y(0) = u_y(0) = 0$. In the computations, we took $L = 20$. Increasing the value of L did not change the results. This problem is precisely equivalent to finding an stripe equilibrium for (1.1) on a domain $[-1, 1]$ with $\varepsilon_0 = 1/L = 0.05$. In the weak interaction regime $D_0 = O(1)$, where both variables are localized, the solution to (6.17) is insensitive to the length L of the interval, provided it is sufficiently large. At each point on this path, the stability of this solution for (1.1) to either breakup or zigzag perturbations is determined by the spectrum of the eigenvalue problem

$$\Phi_{yy} - (1+\mu)\Phi + 2AUV\Phi + AV^2 N = \lambda\Phi\,, \qquad D_0 N_{yy} - (1 + D_0\mu)\,N - 2UV\Phi - V^2 N = \lambda N\tau\,. \tag{6.20}$$

Here $\mu \equiv \varepsilon_0^2 m^2$, and in the computations below we take $\tau = 1.0$. By discretizing (6.20) on the long interval

$[0, L]$, we obtain the block matrix eigenvalue problem

$$\begin{pmatrix} \mathcal{M} - (1+\mu)I + A\Lambda_2 & A\Lambda_1 \\ -\Lambda_2 & D_0\mathcal{M} - (1+D_0\mu)I - \Lambda_1 \end{pmatrix} \begin{pmatrix} \Phi \\ N \end{pmatrix} = \lambda \begin{pmatrix} I & 0 \\ 0 & \tau I \end{pmatrix} \begin{pmatrix} \Phi \\ N \end{pmatrix}. \tag{6.21}$$

For breakup instabilities, $\mathcal{M}$, Λ_1, and Λ_2 are as defined in (3.34). For zigzag instabilities, $\mathcal{M}$ has a slightly different structure than in (3.34). The eigenvalues of (6.21) are computed using a generalized eigenvalue problem solver from LAPACK [**1**] and a quasi-Newton method is used to calculate the instability thresholds.

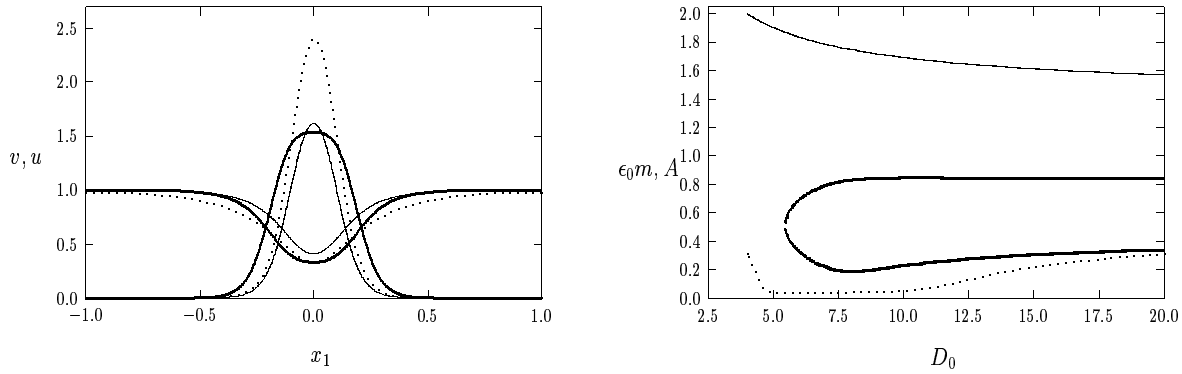

(a) u, v versus x_1 (b) $\varepsilon_0 m$ versus D_0

FIGURE 9. Left figure: plots of u and v, which has a maximum at $x_1 = 0$, for $(D_0, A) = (19.91, 1.57)$ (dashed curve), $(D_0, A) = (5.94, 1.84)$, (solid curve), and $(D_0, A) = (4.0, 2.0)$ (heavy solid curve). Right figure: plots of the breakup instability thresholds (heavy solid curves) and the upper zigzag instability threshold (dashed curve). The top solid curve is the variation of the feed-rate parameter A. The breakup instability band disappears when $D_0 = 5.46$ and $A = 1.87$.

In Fig. 9(a) we plot the solution to (6.17) for three values of D_0. This figure shows that the effect of the finite domain is insignificant in the weak interaction regime. As D_0 decreases, the peak for v decreases and then the region near the peak becomes broader. This flattening of the peak for $D_0 = 4$ is related to the existence of a new spatially inhomogeneous equilibrium solution for v, given by $v_h = \left[\frac{A}{2}\left(1 \pm \sqrt{1 - 4A^{-2}}\right)\right]^{-1}$ that emerges when $A = 2$. In Fig. 9(b) we plot the breakup instability thresholds together with the upper bound of the zigzag band. On the infinite interval the lower bound for the zigzag band is at the origin, since $\lambda = 0$ is an eigenvalue when $m = 0$ that corresponds to the odd translation eigenfunction. Our results show that there is one positive real eigenvalue in the breakup instability band, but that this band terminates at $(A, D_0) = (1.87, 5.46)$. The upper zigzag threshold increases significantly below this value yielding a large range of unstable modes for $D_0 = 4$.

These results show that a stripe can be stabilized in the weak interaction regime with respect to breakup instabilities by the disappearance of the instability band. A similar phenomenon was suggested in §5 of [**7**] for the classical GM model (6.10) in the weak interaction regime. For the GS model, the existence of a zigzag instability band for $D_0 \approx 4$ and $A \approx 2$, without a breakup instability band, is presumably closely related to the

widening of the homoclinic stripe profile as D_0 is decreased. In this range, the stability properties of a stripe are more closely related to those of a front-back transition-layer solution to a bistable system (cf. [**10**]).

An important remark, is that (6.17) also arises as the leading-order problem for the profile of a stripe solution of (1.1) of non-constant curvature, provided that the curvature is $O(1)$ as $\varepsilon_0 \to 0$. In this context, where u and v concentrate along some closed curve $\mathcal{C}$ in the plane, y represents a magnified (by $O(\varepsilon_0^{-1})$) distance perpendicular to $\mathcal{C}$ and the eigenvalue problem (6.20) gives the stability properties of the stripe profile for a mode of the form $e^{\lambda t + ims}\Phi(y)$, where s denotes arclength along $\mathcal{C}$. An unstable mode of integer k is related to m by $m = 2\pi k/L$, where L is the length of $\mathcal{C}$. In the absence of a breakup instability, it is shown numerically in §7 that a zigzag instability of a stripe is the precursor to a labyrinthine pattern. The temporal development of this pattern ultimately terminates when, either, the curvature of the stripe is $O(\varepsilon_0^{-1})$, distant portions of the stripe in terms of arclength become $O(\varepsilon_0)$ close in physical space, or when the stripe becomes $O(\varepsilon_0)$ close to the boundary.

7 Numerical Experiments

We now give some numerical examples to support our analytical results for zigzag and breakup instabilities. The numerical computations for (1.3) were done with the software package "VLUGR" [**3**], which uses an adaptive mesh-refinement algorithm to capture localized structures without an excessive number of meshpoints.

Experiment 1: (Zigzag Instability of a Stripe: One Mode) We consider a stripe equilibrium for (1.3) with $\varepsilon = 0.004$, $A = 1.7069$, and $\tau = 1.0$, in the rectangular domain $[-1,1] \times [0,1]$ so that $d = l = 1$. For $A = 1.7069$, we compute $B = A\tanh 1 = 1.3$. Therefore, this parameter set corresponds to the high feed-rate regime just below the self-replication threshold $B = 1.347$. From the second to last row of Table 1 we get $\sqrt{\mu_1} = 0.339$, $\sqrt{\mu_2} = 0.914$, $m_{0z} = 0.719$, and from Fig. 3 we get $m_{zs} = 1.06$. Therefore, the high feed-rate instability zones from the third row of Table 3 become

$$27.0 < k < 72.8\,, \quad \text{(Unstable Breakup Band)}\,; \qquad 0.34 < k < 57.1\,, \quad \text{(Unstable Zigzag Band)}\,. \tag{7.1}$$

We take a zigzag initial condition for (1.3) of the form $v = \frac{1}{\varepsilon} w\left(\frac{x_1 + 10^{-4}\cos(10\pi x_2)}{\varepsilon}\right)$ and $u = \varepsilon$, where $w(y) = \frac{3}{2}\mathrm{sech}^2(y/2)$. Therefore, there is an initial preference for a zigzag instability corresponding to $k = 10$, or equivalently $m = 10\pi$, which is inside the instability zone. The resulting numerical solution shown in Fig. 10, with five main crests, confirms that the GS model does indeed develop a zigzag instability for this mode.

Numerically, we can also validate the theoretically predicted form of the zigzag instability. From the theory of §3, we would expect that, in terms of the equilibrium stripe solution v_e, the eigenfunction ϕ has the form $\phi = v_e'(x_1)\cos(mx_2)$. Since $v \sim v_e + Ce^{\lambda t}\phi$, it follows that ϕ is well-approximated by the difference in the numerical solution at two neighboring times. In Fig. 11 we plot $v_{t=22} - v_{t=18}$ obtained from our numerical computations. From this figure we observe that the shape of the resulting perturbation is indeed of the form (3.8). The onset of a breakup instability for this example is visible in Fig. 10 at time $t = 32$, when the wiggled stripe starts to develop an instability. Shortly after this time, the stripe breaks up into spots, which then self-replicate until the entire rectangle is full of spots.

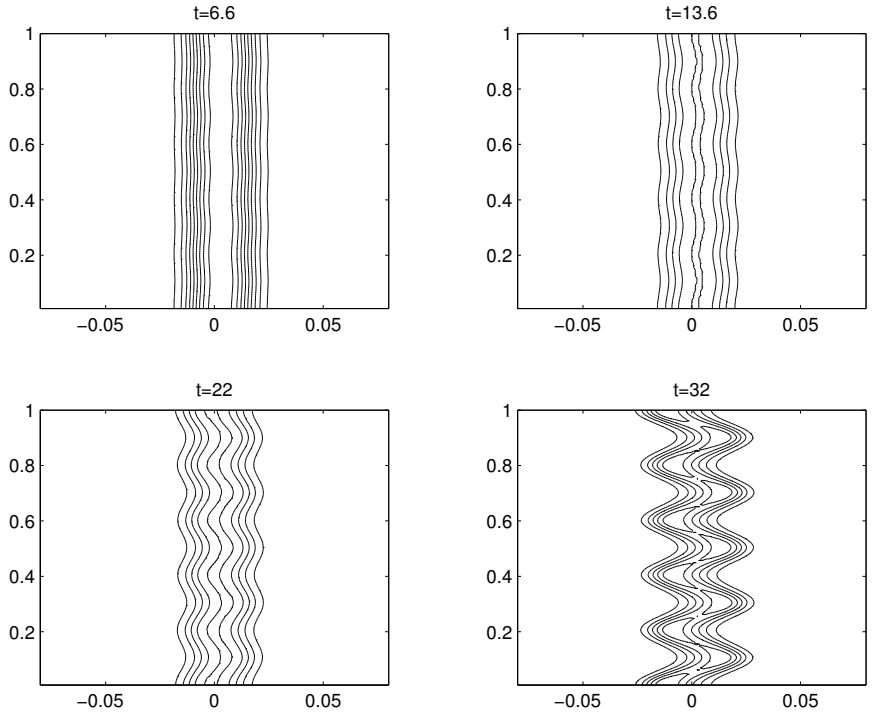

FIGURE 10. **Experiment 1:** Contour plot of v computed from the full numerical solution of (1.3) with $\varepsilon = 0.004$, $A = 1.7069$, and $\tau = 1.0$. The domain is $[-1,1] \times [0,1]$, but we only plot the solution in a thin vertical strip near the centerline. The initial condition is $v = \frac{1}{\varepsilon} w\left(\frac{x_1 + 10^{-4}\cos(10\pi x_2)}{\varepsilon}\right)$, and $u = \varepsilon$, where $w(y) = \frac{3}{2}\mathrm{sech}^2(y/2)$.

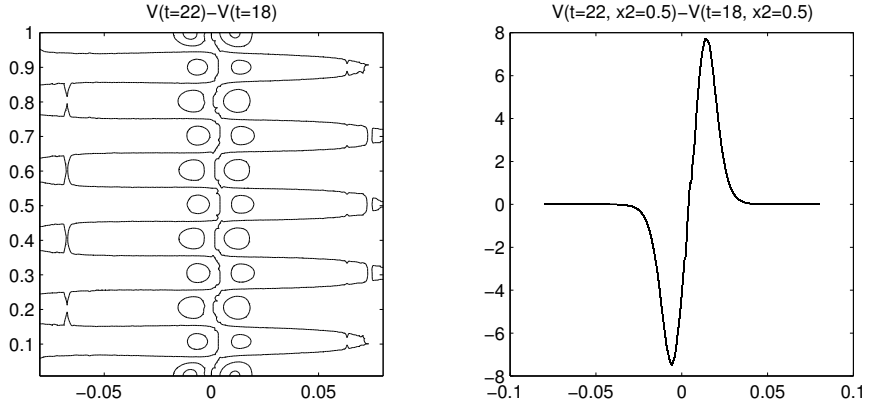

FIGURE 11. **Experiment 1:** Left figure: contour plot of $v_{t=22} - v_{t=18}$ for the data of Fig. 10. Right figure: the horizontal slice of the figure on the left at $x_2 = 0.5$.

Experiment 2: (Breakup Instability of a Stripe: Lower Threshold) Next, we consider an equilibrium stripe solution for (1.3) with $\varepsilon = 0.004$, $A = 1.313$, $\tau = 1.0$, $l = 1$, and $d = 2$. Thus, $\Omega = [-1,1] \times [0,2]$. For $A = 1.313$, we compute $B = A\tanh 1 = 1.0$. From Table 1 and Fig. 5(a) we get $\sqrt{\mu_1} = 0.258$, $\sqrt{\mu_2} = 0.960$,

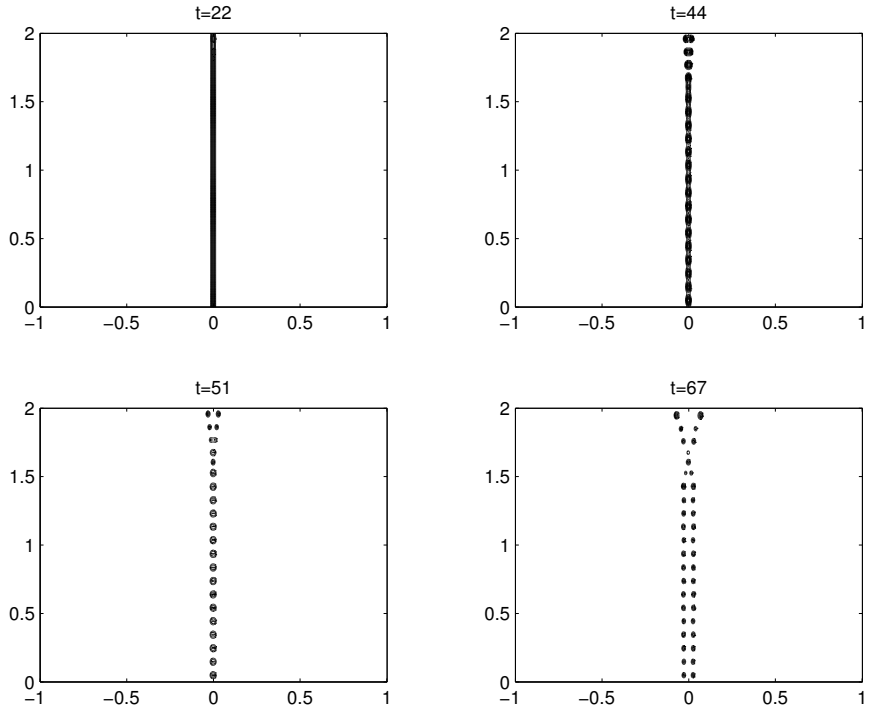

FIGURE 12. **Experiment 2:** Contour plot of v computed from the numerical solution of (1.3) with $\varepsilon = 0.004$, $A = 1.313$, and $\tau = 1.0$. The domain is $[-1,1] \times [0,2]$. The initial condition is given in (7.3).

$m_{0z} = 0.455$, and from Fig. 3 we get $m_{zs} = 1.06$. Therefore, the third row of Table 3 yields

$$40.8 < k < 152.7\,, \quad \text{(Unstable Breakup Band)}\,; \qquad 0.68 < k < 72.1\,, \quad \text{(Unstable Zigzag Band)}\,. \tag{7.2}$$

In this experiment we will verify the lower threshold for breakup instabilities. We take the initial condition

$$v = \frac{1}{\varepsilon}\left[1 + (10^{-4})\cos\left(\frac{40\pi x_2}{2}\right)\right] w\left(x_1/\varepsilon\right)\,, \qquad u = \varepsilon\,, \qquad w(y) \equiv \frac{3}{2}\mathrm{sech}^2(y/2)\,. \tag{7.3}$$

Since $k = 40$, this mode is stable, but is just below the lower instability threshold. In the resulting simulation shown in Fig. 12, the stripe breaks up into 41 and not 40 spots, which lies just within the instability band.

Experiment 3: (Instabilities of a Stripe) We now show breakup and zigzag instabilities for multi-mode initial conditions, we test the critical domain width prediction of §6, and we show stripe self-replication behavior. **Case 1:** Consider a stripe solution for (1.3) with $\varepsilon = 0.02$, $A = 1.7069$, and $\tau = 1.0$, in the rectangular domain $[-1,1] \times [0,1]$ so that $d = l = 1$. For $A = 1.7069$, we compute $B = A\tanh 1 = 1.3$. The threshold values $\sqrt{\mu_1} = 0.339$, $\sqrt{\mu_2} = 0.914$, $m_{0z} = 0.718$, and $m_{zs} = 1.06$ are the same as in Experiment 1. The high feed-rate instability zones calculated from the third row of Table 3 are

$$5.4 < k < 14.5\,, \quad \text{(Unstable Breakup Band)}\,; \qquad 0.34 < k < 11.4\,, \quad \text{(Unstable Zigzag Band)}\,. \tag{7.4}$$

From Fig. 4(b) and Fig. 5(b) we estimate the most unstable zigzag and breakup mode as $\varepsilon m \approx 0.35$ and $\varepsilon m \approx 0.60$, respectively. This gives the most unstable modes $k_z \approx 5.6$ and $k_b \approx 9.5$. The initial condition for

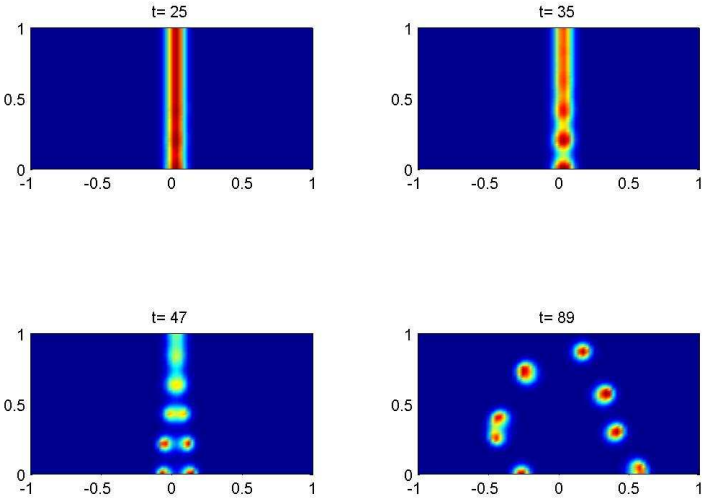

FIGURE 13. **Experiment 3 (Case 1):** Contour plot of v computed from (1.3) with $\varepsilon = 0.02$, $A = 1.7069$, $d = l = 1$, and $\tau = 1.0$. The domain is $[-1, 1] \times [0, 1]$. The initial condition is the breakup form (7.5) with $v_m = 20.11$, $u_m = 0.032$, $j_l = 4$, $j_u = 16$, and $\delta = 10^{-4}$. The stripe breaks into eight spots.

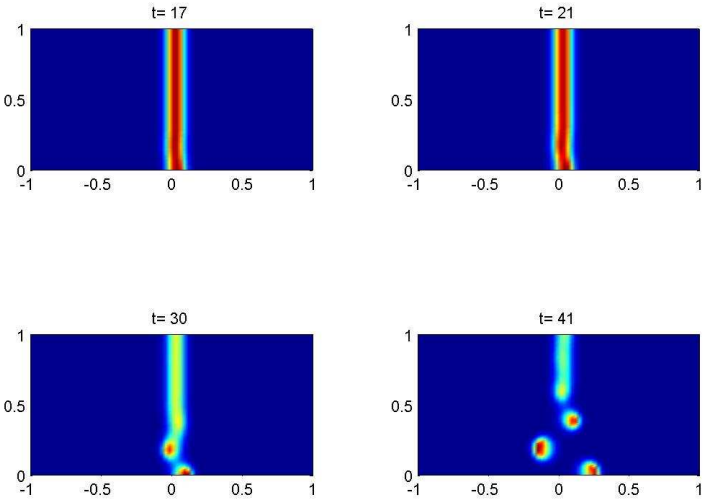

FIGURE 14. **Experiment 3 (Case 2):** Same parameter values as in Fig. 13 except that now the initial condition has the zigzag form (7.6) with $v_m = 20.11$, $u_m = 0.032$, $j_l = 1$, $j_u = 12$, and $\delta = 10^{-4}$. The stripe develops a slight zigzag instability and then breaks up into spots.

the numerical solution of (1.3) is the multi-mode breakup form

$$v = v_m \mathrm{sech}^2\left(\frac{x_1}{2\varepsilon}\right)\left[1+\delta\sum_{j=j_l}^{j_u}\cos\left(j\pi x_2\right)\right], \qquad u = 1-(1-u_m)\,\frac{\cosh(1-|x_1|)}{\cosh 1}. \tag{7.5}$$

We take $\delta = 10^{-4}$, with $j_l = 4$ and $j_u = 16$ to cover the entire breakup instability zone in (7.4). The values $v_m = 20.11$ and $u_m = 0.032$ are obtained from (2.14) and the numerical solution to the core problem (2.3 a) with $B = 1.3$. In Fig. 13 we plot the numerical solution to (1.3). The stripe is found to break into eight spots, which is close to the most unstable mode.

Case 2: We take the same parameters as in Case I, but we replace the initial condition (7.5) with the multi-mode zigzag form

$$v = v_m \mathrm{sech}^2\left[\frac{1}{2\varepsilon}\left(x_1-\delta\sum_{j=j_l}^{j_u}\cos\left(\pi j x_2\right)\right)\right], \qquad u = 1-(1-u_m)\,\frac{\cosh(1-|x_1|)}{\cosh 1}. \tag{7.6}$$

We choose $j_l = 1$ and $j_u = 12$ to cover the entire zigzag band in (7.4), and we take $\delta = 10^{-4}$. In contrast to Experiment 1, some of the zigzag modes in (7.6) lie within the breakup instability band in (7.4). The resulting numerical solution of (1.3) is shown in Fig. 14. The stripe develops a slight zigzag instability, but then quickly disintegrates into spots. The zigzag instability for this example is not as pronounced as that in Experiment 1, which started with an unstable zigzag mode that did not lie within the breakup instability band.

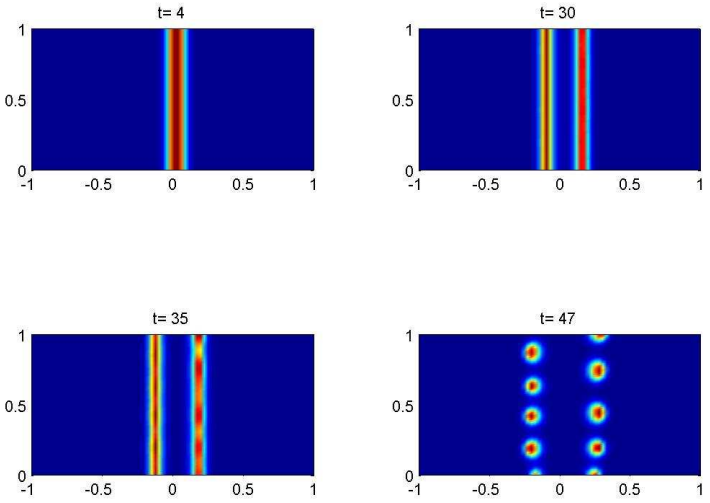

FIGURE 15. **Experiment 3 (Case 3):** Contour plot of v computed from the numerical solution of (1.3) with $\varepsilon = 0.02$, $A = 2.0$, and $\tau = 1.0$. The domain is $[-1, 1] \times [0, 1]$. The initial condition is (7.7) with $v_m = 18.5$ and $u_m = 0.032$. The stripe undergoes a self-replciation event followed by a breakup instability.

Case 3: Next, we take the parameter values $\varepsilon = 0.02$, $A = 2.0$, and $\tau = 1.0$. The domain is $[-1,1] \times [0,1]$. For $A = 2.0$, we compute $B = A \tanh 1 = 1.523$, which exceeds the self-replication threshold $B = 1.347$. The initial condition for (1.3) is taken to be

$$v = v_m \mathrm{sech}^2 \left[x_1/(2\varepsilon) \right] , \qquad u = 1 - (1 - u_m) \frac{\cosh(1 - |x_1|)}{\cosh 1} , \tag{7.7}$$

with $v_m = 18.5$ and $u_m = 0.032$. The numerical solution of (1.3) is shown in Fig. 15. The stripe self-replicates and the two resulting stripes then undergo a breakup instability at a later time leading to a spot pattern.

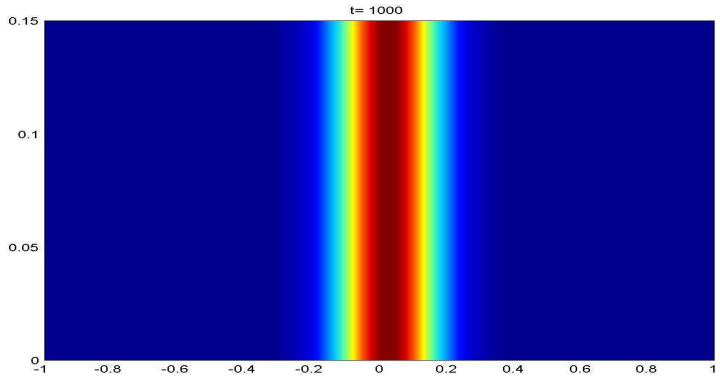

FIGURE 16. **Experiment 3 (Case 4):** Contour plot of v computed from the numerical solution of (1.3) with $\varepsilon = 0.05$, $A = 1.7069$, $l = 1$, $d = 0.15$, and $\tau = 1.0$. The domain is $[-1,1] \times [0, 0.15]$. The initial condition is given in (7.7) with $v_m = 8.04$ and $u_m = .022$. The stripe is stable. The vertical axis is shown in magnified form.

Cases 4 and 5: In this example we test the critical domain width for a breakup instability as predicted in §6. We take the parameter values $\varepsilon = 0.05$, $A = 1.7069$, $l = 1$, and $\tau = 1.0$. Since $\sqrt{\mu_2} = 0.914$, we predict from (6.2) that there will no breakup instabilities for (1.3) when the domain width d satisfies

$$d < d_{0sb}^{\mathrm{h}} = 0.17 . \tag{7.8}$$

The initial condition for (1.3) was taken to be (7.7) with $v_m = 8.04$ and $u_m = 0.022$. The resulting numerical solution of (1.3) in the domain $[-1,1] \times [0, 0.15]$ is shown in Fig. 16. Since $d = 0.15 < d_{0sb}^{\mathrm{h}}$, no breakup instability of the stripe is observed. In Fig. 17 we plot the numerical solution of (1.3) in the wider domain $[-1,1] \times [0, 0.2]$. Since only the $k = 1$ mode is unstable for $d = 0.2$, the stripe is found to disintegrate into exactly one spot.

Experiment 4: (Instabilities of a Ring) Next, we consider an equilibrium ring solution for (1.3) inside the unit circle $R = 1$ with $\varepsilon = 0.04$, $A = 3.871$, and $\tau = 1.0$. Since $D = 1/R^2 = 1$, we get $\rho_0 = 0.712$ from the third row of Table 2. Then, from the data used to generate Fig. 8(a) we obtain $B = A/[2\rho_0 J_1(\rho_0) J_2(\rho_0)] = 1.3$. Therefore, we get the same thresholds $\sqrt{\mu_1} = 0.339$, $\sqrt{\mu_2} = 0.914$, and $m_{0z} = 0.719$, as in Experiment 1. From the third row of Table 2 we get $m_{zr} = 3$. Therefore, from the first row of Table 3, we obtain the instability zones

$$6.04 < m < 16.3 , \quad \text{(Unstable Breakup Band)} ; \qquad 3.0 < m < 12.8 , \quad \text{(Unstable Zigzag Band)} . \tag{7.9}$$

The most unstable breakup modes again correspond roughly to the middle of the breakup band. The initial

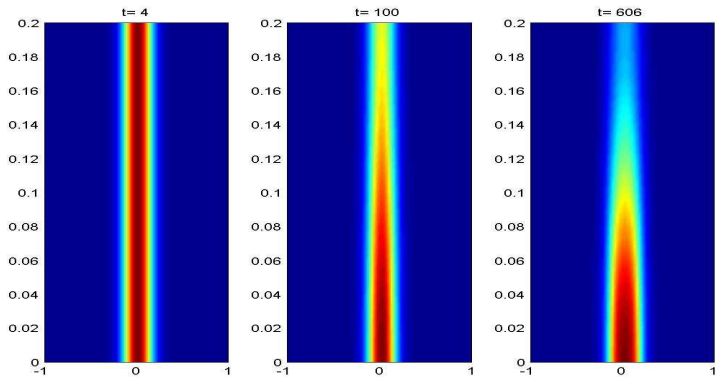

FIGURE 17. **Experiment 3 (Case 5):** Contour plot of v computed from the numerical solution of (1.3) with the same parameters and initial condition as in Fig. 16, except that the domain width is increased to $d = 0.20$. The stripe breaks up into one spot. The vertical axis is shown in magnified form.

condition for (1.3) is taken to have the breakup form

$$v = v_m \mathrm{sech}^2\left(\frac{(r-\rho_0)}{2\varepsilon}\right)\left[1+\delta\sum_{j=5}^{16}\cos(j\theta)\right], \qquad u = 1-(1-u_m)\,\mathrm{sech}^2\left(\frac{(r-\rho_0)}{2\varepsilon}\right), \tag{7.10}$$

with $v_m = 10.0$, $u_m = .028$, and $\delta = 10^{-4}$. Notice that the multi-mode initial condition contains the entire breakup band. In Fig. 18 we plot the numerical solution to (1.3) at different times. The ring is shown to have a breakup instability on an $O(1)$ time-scale, which leads to ten spots. Three of the spots then undergo a secondary instability involving a self-replication process. The final pattern has thirteen spots.

Next, we decrease ε by a factor of two to $\varepsilon = 0.02$. The other parameters are the same as given above. Since the two bounds for the breakup instability are doubled, as well as the upper zigzag instability bound, we get

$$12.1 < m < 32.6\,, \quad \text{(Unstable Breakup Band)}\,; \qquad 3.0 < m < 25.6\,, \quad \text{(Unstable Zigzag Band)}\,. \tag{7.11}$$

From Fig. 5(b) we estimate the most unstable breakup mode as $m_u \approx 22$. The initial condition for (1.3) is taken to have the single-mode zigzag form

$$v = v_m \mathrm{sech}^2\left(\frac{[r-\rho_0\,(1+\delta\cos(10\theta))]}{2\varepsilon}\right), \qquad u = 1-(1-u_m)\,\mathrm{sech}^2\left(\frac{(r-\rho_0)}{2\varepsilon}\right), \tag{7.12}$$

with $\delta = 0.005$. Notice that the initial zigzag mode is not within the breakup instability band. In Fig. 18 we plot the numerical solution to (1.3) at two different times. At short times the solution develops a clear zigzag instability to the $m = 10$ mode. However, at longer times, the wriggled ring eventually undergoes a breakup instability into twenty spots, which is close to the most unstable mode for a breakup instability.

Experiment 5: (Breakup Instabilities of a Ring: Intermediate Regime) Next, we consider instabilities of a ring in the intermediate regime. For (1.3) we take $A = \sqrt{2}$, $R = \sqrt{2}$, and $\varepsilon = 0.0632$. Since $D = 1/R^2 = 0.5$, we get from the fifth row in Table 2 that $\rho_0 = 1.0138$. Then, from the data used to generate Fig. 8(a), we obtain $B = \frac{A}{2\rho_0 J_1(\rho_0)J_2(\rho_0)} = 0.638$, which is well below the existence threshold $B = 1.347$ of the core problem. By

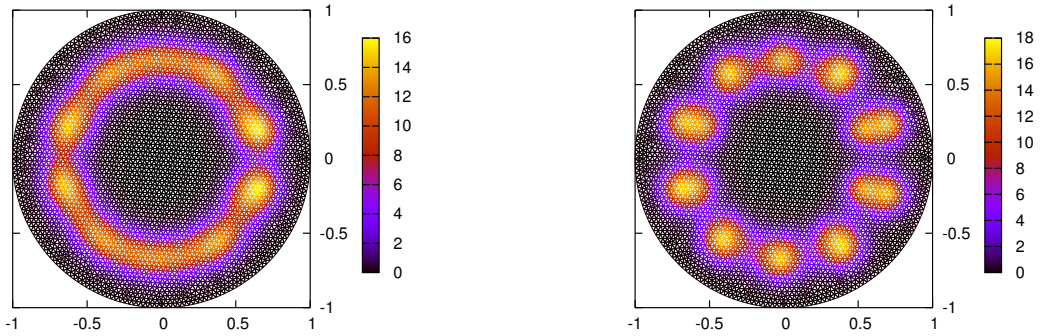

(a) $t = 20$ (b) $t = 35$

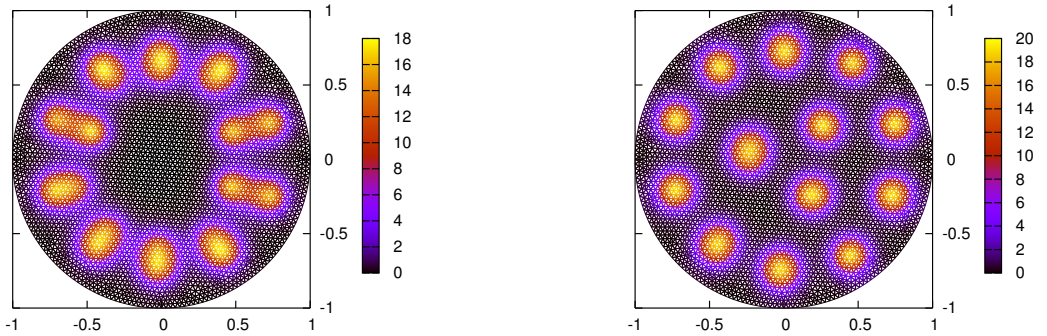

(c) $t = 45$ (d) $t = 105$

FIGURE 18. **Experiment 4 (Breakup):** Contour plot of v computed from the numerical solution of (1.3) in the unit circle with $\varepsilon = 0.04$, $A = 3.871$, and $\tau = 1$. The initial condition is the multi-mode breakup form (7.10). A breakup instability leads to ten spots. A secondary instability of spot-replication leads to a final pattern of thirteen spots.

using the intermediate regime results in the second row of Table 3, we obtain the instability bands

$$2.2 < m < 17.9\,, \quad \text{(Unstable Breakup Band)}\,; \qquad 3.0 < m < 4.4\,, \quad \text{(Unstable Zigzag Band)}\,. \tag{7.13}$$

The zigzag band is very narrow. Fig. 5(b) with $B = 0.638$ gives the most unstable breakup mode as $\varepsilon m \approx 0.4$, which yields $m \approx 7$. A numerical simulation of (1.3) (not shown) with a multi-mode initial condition shows that the ring breaks up into eight spots. As discussed in Appendix B, this example is equivalent to one in [**28**]. As a remark, if for the first example in Experiment 4 we used the intermediate regime breakup instability band in Table 3, instead of the high feed-rate band, we would get the band $10.1 < m < 19.9$. This incorrect band does not contain the unstable $m = 10$ mode observed in Fig. 18.

Experiment 6: (Weak Interaction Regime) Next, we compute solutions to (1.1) in the weak interaction regime with $\varepsilon_0 = 0.02$, $D = 6.08\varepsilon_0^2$ (i.e. $D_0 = 6.08$), $A = 1.83$, and $\tau = 1.0$ in the domain $\Omega = [-1, 1] \times [0, 2]$. The initial condition for (1.1) chosen below is taken to be a close fit to the solution of (6.17) of §6. As mentioned in

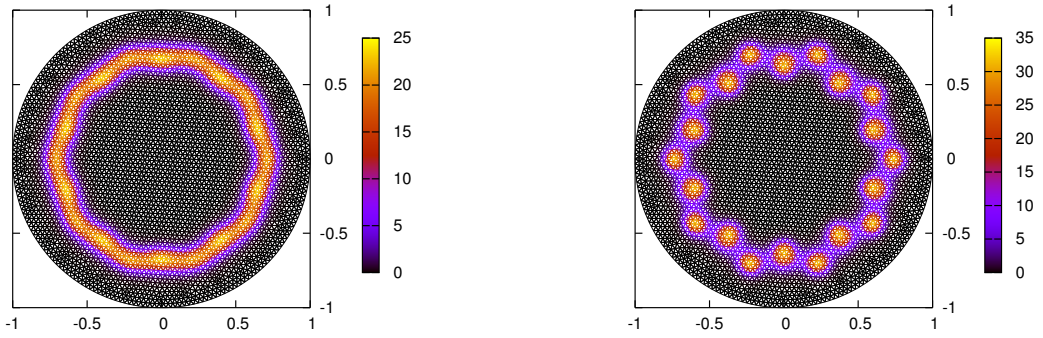

(a) $t = 15$ (b) $t = 25$

FIGURE 19. **Experiment 4 (Breakup and Zigzag):** Contour plot of v computed from the numerical solution of (1.3) in the unit circle with $\varepsilon = 0.02$, $A = 3.871$, and $\tau = 1$. The initial condition is the single-mode zigzag form (7.12). The solution develops a zigzag instability for this mode. The wriggled ring then breaks up into twenty spots.

§6, the solution in Fig. 9(a) gives the profile of a stripe of non-constant curvature in the weak interaction regime. The instability bands in Fig. 9(b) pertain to the stability of this stripe profile. With $v_m = 1.61$, $u_m = 0.414$, and $|x - \eta(\theta)| \equiv \left[(x_1 - \eta_1)^2 + (x_2 - \eta_2)^2\right]^{1/2}$, the precise initial condition for (1.1) is taken to be

$$v(x_1, x_2, 0) = v_m \operatorname{sech}^2\left[\frac{|x - \eta(\theta)|}{5\varepsilon_0}\right], \qquad u(x_1, x_2, 0) = 1 - (1 - u_m)\operatorname{sech}^2\left[\frac{|x - \eta(\theta)|}{4\varepsilon_0}\right]. \tag{7.14 a}$$

Here the triangular-shaped curve $\eta = \eta(\theta)$, with $0 \le \theta < 2\pi$, is given by

$$\eta_1 = \beta(\theta)\cos\theta - \beta'(\theta)\sin\theta\,, \qquad \eta_2 = \frac{3}{4} + \beta(\theta)\sin(\theta) + \beta'(\theta)\cos\theta\,; \qquad \beta(\theta) = \frac{1}{2} + \frac{1}{4}\sin^3(\theta)\,. \tag{7.14 b}$$

In Fig. 20, where we plot the numerical solution to (1.1), we show that the triangular-shaped ring undergoes a breakup instability leading to twelve spots. To explain this, we observe from Fig. 9(b) that there is a breakup instability band for $D_0 = 6.08$, which satisfies $0.316 < \varepsilon_0 m < 0.703$, where $m = 2\pi k/L$ and $L \approx 3.14$ is the numerically computed length of $\eta = \eta(\theta)$. The most unstable mode is roughly in the center of this band so that $2\pi\varepsilon_0 k/L \approx 0.51$. With $\varepsilon_0 = 0.02$ and $L \approx 3.14$ we get $k \approx 12$, which is the number of spots observed in Fig. 20.

Finally, we take $\varepsilon_0 = 0.02$, $A = 2$, $D = 4\varepsilon_0^2$, $v_m = 1.54$, and $u_m = 0.33$. The initial condition for (1.1) is again given by (7.14). For these values of A and $D_0 = 4$ we recall from Fig. 9(b) that there is only a zigzag instability band, and that the solution should be stable to breakup instabilities. From Fig. 9(b) the most unstable zigzag mode is roughly in the middle of the band so that $\varepsilon_0 m \approx 0.2$. With $m = 2\pi k/L$, and $L \approx 3.14$, we get $k \approx 5$. In Fig. 21 we plot the full numerical solution to (1.1) showing the initial development of a $k = 6$ zigzag instability, and the subsequent temporal development of a large-scale labyrithinian pattern.

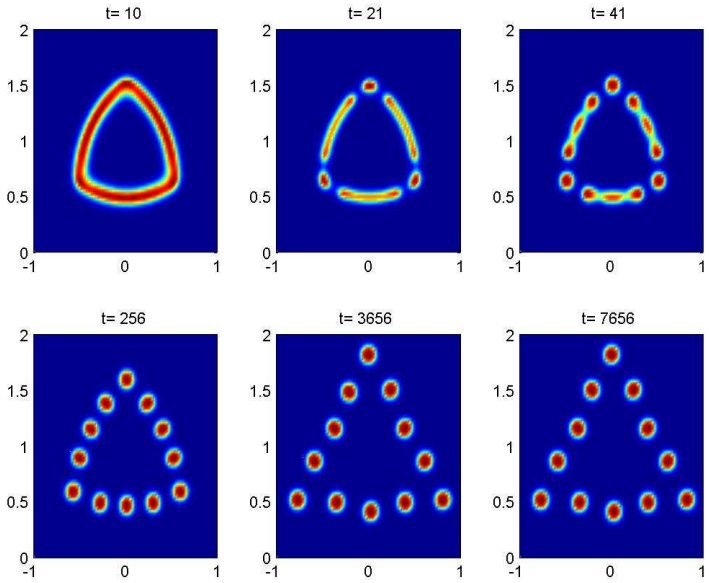

FIGURE 20. **Experiment 6a:** (Weak Interaction Regime: Breakup Instability) Contour plot of the solution v to (1.1) with $\varepsilon_0 = 0.02$, $D = 6.08\varepsilon_0^2$, $A = 1.83$, and $\tau = 1.0$, at different times. The initial condition is given in (7.14) with $v_m = 1.61$ and $u_m = 0.414$. The triangular-shaped ring breaks up into twelve spots.

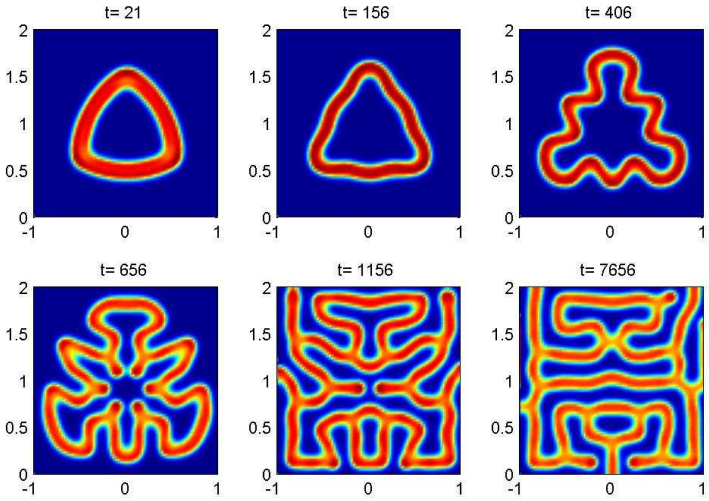

FIGURE 21. **Experiment 6b:** (Weak Interaction Regime: Zigzag Instability) Contour plot of the solution v to (1.1) with $\varepsilon_0 = 0.02$, $D = 4\varepsilon_0^2$, $A = 2.0$, and $\tau = 1.0$, at different times. The initial condition is (7.14) with $v_m = 1.54$ and $u_m = 0.33$. No breakup instability occurs, and the zigzag instability is seen to be the precursor to a large-scale labyrinthine pattern.

8 Conclusion

We have analyzed zigzag and breakup instabilities of stripes and rings for the GS model (1.3) in the semi-strong interaction regime where only the v component is localized. In this regime we calculated instability bands for both types of instabilities. The two instability bands have been determined for both the high feed-rate regime $A = O(1)$ and the intermediate regime $O(\varepsilon^{1/2}) \ll A \ll O(1)$. We have shown that the two instability bands overlap in such a way that, for an arbitrary initial perturbation, a zigzag instability is always accompanied by a breakup instability. A stripe can be stable with respect to zigzag and breakup instabilities only when the domain width d_0 is $O(\varepsilon)$ small. Although our analysis determines the conditions for the onset of the instabilities in terms of the parameters in the GS model, an open problem is to provide a weakly nonlinear theory for their development and interaction. Another open problem is to analyze zigzag and breakup instabilities of multi-stripe and multi-ring equilibria. Such equilibria occur after a stripe or ring self-replication event.

An important open problem is to study the transition from the semi-strong to the weak-interaction regime with regards to both the bifurcation diagram of equilibrium stripe solutions and to determining precise instability bands for zigzag and breakup instabilities. The weak interaction regime corresponds to the limit $l \gg 1$ and $\varepsilon = O(1)$ in the GS model (1.3). In this regime, both u and v are localized near a stripe or ring. Pattern formation and pulse-splitting behavior in this regime was studied in [**33**], [**34**], and [**42**], for the special case $\varepsilon = 1/2$. The numerical eigenvalue computations of §6 and the numerical simulation in Experiment 6 in §7 indicate that there exists parameter values where a stripe or ring is stable with respect to breakup instabilities, but is unstable with respect to zigzag instabilities. In the weak interaction regime, we conjecture that in the absence of such breakup instabilities a zigzag instability leads to a labyrinthine pattern such as shown in Fig. 21.

Finally, it would be interesting to extend the stability analyses given here to investigate breakup and zigzag instabilities of stripes and rings in the hybrid chemotaxis reaction-diffusion systems of [**41**], [**48**], [**35**], and [**36**].

Appendix A Stripe Stability for the Gray-Scott Model in the Low Feed Rate Regime

In this appendix, we give a brief outline of the derivation of Principal Result 6.1 for the stability of a stripe for the GS model (1.3) in the rectangular domain $\Omega = [-l, l] \times [0, ld_0]$ in the low feed-rate regime $A = O(\varepsilon^{1/2})$. In the low feed-rate regime, we introduce ν and $\mathcal{A}$ by $A = \varepsilon^{1/2}\mathcal{A}$ and $v = \varepsilon^{-1/2}\nu$. Then, (1.3) becomes

$$\nu_t = \varepsilon^2 \Delta\nu - \nu + \mathcal{A} u \nu^2\,, \quad \tau u_t = \Delta u - u + 1 - \varepsilon^{-1} u\nu^2\,, \quad x = (x_1, x_2) \in \Omega\,; \quad \partial_n u = \partial_n \nu = 0\,, \quad x \in \partial\Omega\,. \tag{A.1}$$

For $\varepsilon \ll 1$, a matched asymptotic analysis leads to two equilibrium stripe solutions of the form

$$\nu_\pm(x_1) \sim \frac{1}{\mathcal{A} U_\pm} w\left[\varepsilon^{-1} x_1\right]\,, \qquad u_\pm(x_1) \sim 1 - (1 - U_\pm)\frac{G_l(x_1)}{G_l(0)}\,, \qquad U_\pm = \frac{1}{2}\left[1 \pm \sqrt{1 - \frac{\mathcal{A}_{1e}^2}{\mathcal{A}^2}}\right]\,, \tag{A.2 a}$$

where $\mathcal{A}_{1e} = \sqrt{24 G_l(0)}$ is the saddle-node value. Here $w(y)$ is the homoclinic of (2.19) and $G_l(x_1)$, with $G_l(0) = \frac{1}{2}\coth l$, is the Green's function satisfying (2.7). These two solutions are parameterized in terms of s by

$$\mathcal{A} = \mathcal{A}_{1e}\frac{(1+s)}{2\sqrt{s}}\,, \quad 0 < s < \infty\,; \qquad \mathcal{A}_{1e} \equiv \sqrt{12\coth l}\,, \qquad U_\pm \equiv \frac{1}{s+1}\,. \tag{A.2 b}$$

Since u_+, ν_+, corresponding to $0 < s < 1$, is unstable as a pulse in one-dimension (cf. [**18**]), we will only study instabilities of the large solution $u_e \equiv u_-$, $\nu_e \equiv \nu_-$, where $s > 1$. In (A.1) we introduce the perturbation

$$\nu = \nu_e(x_1) + e^{\lambda t + imx_2}\phi(x_1)\,, \qquad u = u_e(x_1) + e^{\lambda t + imx_2}\eta(x_1)\,, \tag{A.3}$$

where $\phi_{x_1}(\pm l) = \eta_{x_1}(\pm l) = 0$. Substituting (A.3) into (A.1), and linearizing, we obtain the eigenvalue problem

$$\varepsilon^2\phi_{x_1x_1} - \phi + 2\mathcal{A}u_e\nu_e\phi + \mathcal{A}\eta\nu_e^2 = \left(\lambda + \varepsilon^2 m^2\right)\phi\,, \quad \eta_{x_1x_1} - \left(1 + m^2 + \tau\lambda\right)\eta = \varepsilon^{-1}\nu_e^2\eta + 2\varepsilon^{-1}u_e\nu_e\phi\,, \quad |x_1| < l\,. \tag{A.4}$$

To study breakup instabilities, we look for a localized eigenfunction of the form $\phi(x_1) = \Phi\left(\varepsilon^{-1}x_1\right)$. By substituting this form and (A.2 *a*) into (A.4), and noting that $\int_{-\infty}^{\infty} w^2\,dy = 6$ and $6/(\mathcal{A}^2U^2) = s/G_l(0)$, we get

$$\Phi'' - \Phi + 2w\Phi + \frac{s\eta(0)}{G_l(0)}\frac{\mathcal{A}w^2}{\int_{-\infty}^{\infty} w^2\,dy} = \left(\lambda + \varepsilon^2 m^2\right)\Phi\,, \quad -\infty < y < \infty\,; \quad \Phi(y) \to 0 \quad |y| \to \infty\,. \tag{A.5}$$

The coefficients in (A.4) are calculated in terms of Dirac masses as in §3 of [**18**]. This leads to the outer problem

$$\eta_{x_1x_1} - \theta_\lambda^2\eta = \left(\frac{s\eta(0)}{G_l(0)} + \frac{2}{\mathcal{A}}\int_{-\infty}^{\infty} w\Phi\,dy\right)\delta(x_1)\,, \quad |x_1| < l\,; \quad \eta_{x_1}(\pm l) = 0\,; \qquad \theta_\lambda \equiv \sqrt{1 + m^2 + \tau\lambda}\,. \tag{A.6}$$

Then, we introduce the Green's function $G_\lambda(x_1)$ satisfying

$$G_{\lambda x_1x_1} - \theta_\lambda^2 G_\lambda = -\delta(x_1)\,, \quad |x_1| < l\,; \qquad G_{\lambda x_1}(\pm l) = 0\,. \tag{A.7}$$

The solution to (A.6) is written in terms of $G_\lambda(x_1)$, and from this solution we calculate $\eta(0)$ as

$$\eta(0)\left(1 + s\frac{G_\lambda(0)}{G_l(0)}\right) = -\frac{2G_\lambda(0)}{\mathcal{A}}\int_{-\infty}^{\infty} w\Phi\,dy\,. \tag{A.8}$$

By substituting (A.8) into (A.5), and using $G_l(0) = \frac{1}{2}\coth l$ and $G_\lambda(0) = (2\theta_\lambda)^{-1}\coth(l\theta_\lambda)$, we obtain the following nonlocal eigenvalue problem on $-\infty < y < \infty$ with $\Phi \to 0$ as $|y| \to \infty$:

$$L_0\Phi - \chi w^2\frac{\int_{-\infty}^{\infty} w\Phi\,dy}{\int_{-\infty}^{\infty} w^2} = (\lambda + \varepsilon^2 m^2)\Phi\,; \qquad C(\lambda) \equiv \frac{1}{\chi(\lambda)} \equiv \frac{1}{2} + \frac{\theta_\lambda\tanh(\theta_\lambda l)}{2s\tanh l}\,, \tag{A.9}$$

where $L_0\Phi \equiv \Phi'' - \Phi + 2w\Phi$. First, let $m = O(1)$. Then, Lemma 4.1 in §4 above, due to [**43**], proves that we have instability for any $\tau > 0$ when $C(0) > 1$. By calculating $C(0)$ explicitly, we obtain the lower instability threshold in (6.7 *a*). Next, let $m = m_0\varepsilon^{-1} \gg 1$. Then, we obtain that $\chi \to 0$ as $\varepsilon \to 0$ for all s in $1 < s < O(\varepsilon^{-1})$, which includes the intermediate regime. Thus, (A.9) reduces to $L_0\Phi = (\lambda + m_0^2)\Phi$. Since $L_0\Psi = \sigma\Psi$ has the unique unstable eigenvalue $\sigma = 5/4$, we set $\lambda = 0$ to get the upper threshold $m = \sqrt{5}/(2\varepsilon)$ in (6.7 *a*).

To analyze zigzag instabilities we must calculate the small eigenvalue $\lambda = O(\varepsilon^2)$ of (A.4). Since a similar analysis was done for multi-spike solutions with $m = 0$ in §3 of [**21**] we omit the intermediate steps of the calculation. The corresponding eigenfunction for ϕ has the form

$$\phi(x_1) = w'\left(\varepsilon^{-1}x_1\right) + \varepsilon\phi_1\left(\varepsilon^{-1}x_1\right) + \cdots\,, \qquad \eta(x_1) = \varepsilon\eta_0(x_1) + \cdots\,. \tag{A.10}$$

By modifying the derivation of Principal Result 3.1 of [**21**], we obtain that the small eigenvalue satisfies

$$\lambda \sim 2\varepsilon^2 s\left[\langle\tilde{\eta}_{0x_1}\rangle - 1\right] - \varepsilon^2 m^2\,. \tag{A.11}$$

Here $\tilde{\eta}_0(x_1)$, related to $\eta_0(x_1)$ by $\eta_0 = -6G_l(0)\tilde{\eta}_0/\mathcal{A}$, satisfies the auxiliary problem

$$\tilde{\eta}_{0x_1x_1} - \theta^2\tilde{\eta}_0 = 0\,, \quad |x_1| < l\,; \qquad \tilde{\eta}_{0x_1}(\pm l) = 0\,; \qquad [\tilde{\eta}_0] = -\frac{1}{G_l(0)}\,, \quad [\tilde{\eta}_{0x_1}] = \frac{-s}{G_l(0)}\langle\tilde{\eta}_0\rangle\,, \tag{A.12}$$

where $\theta \equiv \sqrt{1+m^2}$. Here we have defined the bracket notation as $\langle\zeta\rangle \equiv (\zeta(0^+) + \zeta(0^-))/2$ and $[\zeta] \equiv \zeta(0^+) - \zeta(0^-)$, where $\zeta(0^\pm)$ are the one-sided limits of $\zeta(x_1)$ as $x_1 \to 0^\pm$. By solving (A.12) explicitly, we obtain

$$\langle\tilde{\eta}_{0x_1}\rangle = \theta\tanh(\theta l)\tanh l\,, \qquad \theta \equiv \sqrt{1+m^2}\,. \tag{A.13}$$

Substituting (A.13) into (A.11), we obtain the expression (6.8) for the small eigenvalue in Principal Result 6.1.

Appendix B Breakup Instability of a Ring for the Gray-Scott Model

In [**28**] breakup instabilities of a ring were studied for the GS model in the low feed-rate regime, and some results were given there for the intermediate regime. In addition, ring splitting behavior was computed numerically in [**28**], and Turing patterns were shown to be the final equilibrium state after a ring undergoes a breakup instability. In [**28**] the GS model was written in a disk Ω_{mk} of radius R_{mk} in the form

$$V_T = D_{mk}\Delta V - B_{mk}V + UV^2\,, \qquad U_T = \Delta U - UV^2 + A_{mk}(1-U)\,, \quad X \in \Omega_{mk}\,. \tag{B.1}$$

In terms of our dimensionless groupings of (1.1) for the unit disk, we readily calculate that

$$\tau = \frac{B_{mk}}{A_{mk}}\,, \qquad D = \frac{1}{R_{mk}^2 A_{mk}}\,, \qquad \varepsilon_0 = \sqrt{\frac{D_{mk}}{R_{mk}^2 B_{mk}}}\,, \qquad A = \frac{\sqrt{A_{mk}}}{B_{mk}}\,. \tag{B.2}$$

In terms of (1.3), analyzed in §5 in the disk $|x| < R$, we further identify $\varepsilon = \varepsilon_0/\sqrt{D}$ and $R = 1/\sqrt{D}$, so that

$$\varepsilon = \sqrt{\frac{D_{mk}A_{mk}}{B_{mk}}}\,, \qquad R = R_{mk}\sqrt{A_{mk}}\,. \tag{B.3}$$

For $B_{mk}^3 D_{mk} \ll A_{mk}$, equation (2.37) of [**28**] shows that the equilibrium ring radius ρ_{mk} for (B.1) satisfies

$$\frac{6B_{mk}^{3/2}\sqrt{D_{mk}}}{\sqrt{A_{mk}}} = \frac{2\sqrt{A_{mk}}\rho_{mk}}{L_{mk}^2}\left[-Q_0 + \frac{1}{2}\left(Q_1 - Q_2\right)\right]\,, \tag{B.4}$$

where L_{mk}, Q_0, Q_1, and Q_2, are defined in terms of modified Bessel functions in equations (2.16), (2.21), and (2.33) of [**28**]. To convert (B.4) to our notation we use (B.2) and (B.3). We first identify that

$$\frac{6B_{mk}^{3/2}\sqrt{D_{mk}}}{\sqrt{A_{mk}}} = \frac{6\varepsilon_0}{A^2\sqrt{D}}\,. \tag{B.5}$$

Then, by using (B.2) and (B.3) in (B.4), together with a Wronskian relation between I_0 and K_0, we readily show that the equilibrium ring radius ρ_0 in terms of our formulation (1.3) satisfies

$$\frac{6\varepsilon_0}{A^2\sqrt{D}} = \frac{2I_1(\rho_0)I_0(\rho_0)}{\left[J_1(\rho_0)J_2(\rho_0)\right]^2}\left[-\frac{K_0(\rho_0)}{I_0(\rho_0)} + \frac{K_0'(R)}{I_0'(R)} + \frac{1}{2\rho_0 I_0(\rho_0)I_0'(\rho_0)}\right]\,, \tag{B.6}$$

where $J_1(\rho_0)$ and $J_2(\rho_0)$ are defined in (5.7). In the intermediate regime, where $O(\varepsilon_0^{1/2}) \ll A \ll O(1)$, we can

neglect the left hand-side of (B.6) to show that ρ_0 satisfies the intermediate regime result (5.28) of §5. As a remark, the result (B.6) can also be obtained from the low feed-rate result in Theorem 2.1 of [**22**].

In [**28**] the breakup instability of a ring was studied by first formulating a nonlocal eigenvalue problem (NLEP) and then by computing its instability band using hypergeometric functions. The theoretical breakup instability band in the second row of Table 3 was not identified in [**28**]. Experiment 5 of §7 corresponds to simulation 2 of [**28**] where $A_{mk} = .08$, $B_{mk} = 0.2$, $D_{mk} = .01$, and $R_{mk} = 5$. By using (B.2), (B.3), and (5.28), we compute $A = 1.4142$, $B = \frac{A}{2\rho_0 J_1(\rho_0)J_2(\rho_0)} = 0.638$, $R = \sqrt{2}$, $\varepsilon = 0.0632$, and $\rho_0 = 1.014$. The theoretical ring breakup instability band from the second row of Table 3 gives $2.2 < m < 17.9$. Then, Fig. 5(b) with $B = 0.638$ can be used to estimate the most unstable mode as $\varepsilon m \approx 0.4$, which yields $m \approx 7$. In comparison, the instability zone in Fig. 7 of [**28**] was computed numerically to be $1.6 < m < 14.0$, with the modes $m = 5, 6, 7, 8$ being strongly unstable. Since $\varepsilon = 0.063$ is only moderately small, we remark that if we used the full result (B.6) rather than the intermediate regime result (5.28) to compute ρ_0, we get $\rho_0 = 0.886$. From Table 3, this gives the theoretical breakup instability band $2.4 < m < 15.6$, which compares better with the result of [**28**]. The other examples in the first few rows of Table 2 of [**28**] can be treated similarly.

From numerical computations of the spectrum of the NLEP using hypergeometric functions, it was suggested in Table 2 of [**28**] that the breakup instability band can disappear if the ratio $\gamma_{mk} \equiv A_{mk}^2/\left[36B_{mk}^2 L_{mk}^2\right]$ is sufficiently large. This was done by fixing $A_{mk} = .04$, $D_{mk} = .005$, and $R_{mk} = 5$, and by taking a decreasing sequence of B_{mk} values in the set $\{0.14, 0.12, 0.1, 0.08, 0.06, 0.05, 0.045, 0.040, 0.038\}$. By using (B.6) to compute ρ_0, it was suggested in [**28**] that a ring is stable to breakup instabilities when $B_{mk} < 0.05$, or equivalently when $\gamma_{mk} < 0.22$. However, we argue that this conclusion is incorrect since it is based on extending the analysis in [**28**] beyond its range of validity. In terms of our notation, we use (B.2) and (B.3) to calculate γ_{mk} as

$$\gamma_{mk} \equiv \frac{A^2}{36\left[\rho_0 J_1(\rho_0)J_2(\rho_0)\right]^2} = \frac{B^2}{9}\,. \tag{B.7}$$

By comparing (B.7) with the breakup instability band in the second row of Table 3 we would predict that the breakup band in the intermediate regime disappears when $\gamma_{mk} = \sqrt{5}/6$. However, as discussed in §6, this conclusion is incorrect on two grounds in that it predicts a core parameter $B = A/[2\rho_0 J_1(\rho_0)J_2(\rho_0)]$ that exceeds the ring-splitting threshold $B = 1.347$ of the high feed-rate regime, and this parameter does not lie in the assumed range $O(\varepsilon^{1/2}) \ll B \ll O(1)$. This suggests that the last two rows of Table 2 of [**28**] where $B_{mk} = 0.05$ and $B_{mk} = 0.04$ should correspond to the high feed-rate regime where $B > 1.347$. If we use (B.6) to compute ρ_0, and (B.2) to obtain A, we compute that $B = 1.39$ for $B_{mk} = 0.05$ and $B = 1.724$ for $B_{mk} = 0.04$. Therefore, the last few rows of Table 2 correspond to the ring-splitting regime $B > 1.347$, where there is no equilibrium ring solution.

Acknowledgments. T.K. was supported by a PGS-B graduate scholarship from NSERC Canada. M.J.W. thanks the grant support of NSERC. J.W. is supported by an Earmarked Grant from RGC of Hong Kong. We would like to thank Prof. David Iron of Dalhousie University for his help with setting up the VLUGR code. We are very grateful to Dr. Wentao Sun for the numerical computation of the ring solutions in §7.

References

[1] E. Anderson et al. *LAPACK User's Guide: Third Edition*, SIAM Publications (1999).

[2] M. Abramowitz, I. A. Stegun, *Handbook of Mathematical Functions with Formulas, Graphs, and Mathematical Tables*, Washington, National Bureau of Standards Applied Mathematics, 1964.

[3] J. G. Bom, R. A. Trompert, J. G. Verwer, *Algorithm 758: VLUGR2: A Vectorizable Adaptive Grid Solver for PDEs in 2D*, Association for Computing Machinery Transactions on Mathematical Software, **22**, (1996), pp. 302-328.

[4] A. Bose, G. Kriegsmann, *Large Amplitude Solutions of Spatially Non-Homogeneous Nonlocal Reaction-Diffusion Equations*, Meth. Appl. Anal., **7**, No. 2, (2000), pp. 295-311.

[5] A. Doelman, R. A. Gardner, T. J. Kaper, *Stability Analysis of Singular Patterns in the 1D Gray-Scott Model: A Matched Asymptotics Approach*, Physica D, **122**, No. 1-4, (1998), pp. 1-36.

[6] A. Doelman, T. J. Kaper, P. Zegeling, *Pattern Formation in the One-Dimensional Gray-Scott Model*, Nonlinearity, **10**, No. 2, (1997), pp. 523-563.

[7] A. Doelman, H. van der Ploeg, *Homoclinic Stripe Patterns*, SIAM J. Appl. Dyn. Systems, **1**, No. 1, (2002), pp. 65-104.

[8] S. Ei, Y. Nishiura, K. Ueda, 2^n *Splitting or Edge Splitting?: A Manner of Splitting in Dissipative Systems*, Japan J. Indust. Appl. Math., **18**, (2001), pp. 181-205.

[9] A. Gierer, H. Meinhardt, *A Theory of Biological Pattern Formation*, Kybernetik, **12**, (1972), pp. 30–39.

[10] R. E. Goldstein, D. J. Muraki, D. M. Petrich, *Interface Proliferation and the Growth of Labyrinths in a Reaction-Diffusion System*, Phys. Rev. E., **53**, (1996), pp. 3933-3957.

[11] P. Gray, S. K. Scott, *Autocatalytic Reactions in the Isothermal, Continuous Stirred Tank Reactor: Oscillations and Instabilities in the System* $A + 2B \to 3B$, $B \to C$, Chem. Eng. Sci., **39**, (1984), pp. 1087-1097.

[12] A. Hagberg, E. Meron, T. Passot, *Phase Dynamics of Nearly Stationary Patterns in Activator-Inhibitor Systems*, Phys. Rev. E., **61**, No. 6, (2000), pp. 6471-6476.

[13] P. Hirschberg, E. Knobloch, *Zigzag and Varicose Instabilities of a Localized Stripe Pattern*, Chaos, **3**, (1993), pp. 713-721.

[14] J. K. Hale, L. A. Peletier, W. C. Troy, *Exact Homoclinic and Heteroclinic Solutions of the Gray-Scott Model for Autocatalysis*, SIAM J. Appl. Math., **61**, (2000), pp. 102-130.

[15] B. S. Kerner, V. V. Osipov, *Autosolitions: A New Approach to Problem of Self-Organization and Turbulence*, Kluwer Academic Publishers, Dordrecht, (1994).

[16] A. J. Koch, H. Meinhardt, *Biological Pattern Formation From Basic Mechanisms to Complex Structures*, Rev. Modern Physics, **66**, No. 4, (1994), pp. 1481-1507.

[17] T. Kolokolnikov, M. Ward, J. Wei, *The Existence and Stability of Spike Equilibria in the One-Dimensional Gray-Scott Model: The Pulse-Splitting Regime*, accepted, Physica D., (2005).

[18] T. Kolokolnikov, M. Ward, J. Wei, *The Existence and Stability of Spike Equilibria in the One-Dimensional Gray-Scott Model: The Low Feed-Rate Regime*, accepted, Studies in Appl. Math., (2005).

[19] T. Kolokolnikov, M. J. Ward, J. Wei, *The Stability of a Stripe for the Gierer-Meinhardt Model and the Effect of Saturation*, in preparation.

[20] T. Kolokolnikov, M. J. Ward, J. Wei, *Pulse-Splitting for Some Reaction-Diffusion Systems in One-Space Dimension*, Studies in Appl. Math., **114**, No. 2, (2005), pp. 115-165.

[21] T. Kolokolnikov, M. J. Ward, J. Wei, *Slow Translational Instabilities of Spike Patterns in the One-Dimensional Gray-Scott Model*, submitted, Interfaces and Free Boundaries, (2005).

[22] T. Kolokolnikov, J. Wei, *On Ring-Like Solutions for the Gray-Scott Model: Existence, Instability, and Self-Replicating Regimes*, accepted, Europ. J. Appl. Math., (2004).

[23] K. J. Lee, W. D. McCormick, J. E. Pearson, H. L. Swinney, *Experimental Observation of Self-Replicating Spots in a Reaction-Diffusion System*, Nature, **369**, (1994), pp. 215-218.

[24] K. J. Lee, W. D. McCormick, Q. Ouyang, H. L. Swinney, *Pattern Formation by Interacting Chemical Fronts*, Science, **261**, (1993), pp. 192-194.

[25] C. S. Lin, W. M. Ni, I. Takagi, *Large Amplitude Stationary Solutions to a Chemotaxis System*, J. Diff. Eq., **72**, (1988), pp. 1-27.

[26] W. Mazin, K. E. Rasmussen, E. Mosekilde, P. Borckmans, G. Dewel, *Pattern Formation in the Bistable Gray-Scott Model*, Math. and Computers in Simulation, **40**, (1996), pp. 371-396.

[27] H. Meinhardt, *The Algorithmic Beauty of Sea Shells*, Springer-Verlag, Berlin, (1995).

[28] D. Morgan, T. Kaper, *Axisymmetric Ring Solutions of the Gray-Scott Model and Their Destabilization into Spots*, Physica D, **192**, No. 1-2, (2004), pp. 33–62.

[29] C. Muratov, V. V. Osipov, *Static Spike Autosolitons in the Gray-Scott Model*, J. Phys. A: Math Gen. **33**, (2000), pp. 8893-8916.

[30] C. Muratov, V. V. Osipov, *Stability of the Static Spike Autosolitons in the Gray-Scott Model*, SIAM J. Appl. Math., **62**, No. 5, (2002), pp. 1463-1487.

[31] C. Muratov, V. V. Osipov, *Spike Autosolitons and Pattern Formation Scenarios in the Two-Dimensional Gray-Scott Model*, Eur. Phys. J. B, **22**, (2001), pp. 213-221.

[32] J. D. Murray, *Mathematical Biology II: Spatial Models and Biomedical Applications*, Interdisciplinary Applied Mathematics, Vol. 18, Springer, New York, (2003).

[33] Y. Nishiura, D. Ueyama, *A Skeleton Structure of Self-Replicating Dynamics*, Physica D, **130**, No. 1-2, (1999), pp. 73-104.

[34] Y. Nishiura, D. Ueyama, *Spatio-Temporal Chaos for the Gray-Scott Model*, Physica D, **150**, No. 3-4, (2001), pp. 137-162.

[35] K. J. Painter, P. K. Maini, H. G. Othmer, *Complex Patterns in a Hybrid Chemotaxis Reaction-Diffusion Model*, J. Math. Biology, **41**, No. 4, (2000), pp. 285-314.

[36] K. J. Painter, P. K. Maini, H. G. Othmer, *Stripe Formation in Juvenile Pomacanthus Explained by a Generalized Turing Mechanism with Chemotaxis*, Proc. Natl. Acad. Sci. USA, Developmental Biology, **96**, (1999), pp. 5549-5554.

[37] J. E. Pearson, *Complex Patterns in a Simple System*, Science, **216**, (1993), pp. 189-192.

[38] W. N. Reynolds, S. Ponce-Dawson, J. E. Pearson, *Dynamics of Self-Replicating Patterns in Reaction-Diffusion Systems*, Phys. Rev. Lett., **72**, (1994), pp. 2797-2800.

[39] W. N. Reynolds, S. Ponce-Dawson, J. E. Pearson, *Dynamics of Self-Replicating Spots in Reaction-Diffusion Systems*, Phys. Rev. E, **56**, No. 1, (1997), pp. 185-198.

[40] M. Taniguchi, Y. Nishiura, *Instability of Planar Interfaces in Reaction-Diffusion Systems*, SIAM J. Math. Anal., **25**, No. 1, (1994), pp. 99-134.

[41] R. C. Tyson, *Pattern Formation by E. Coli; Mathematical and Numerical Investigation of a Biological Phenomenon*, Ph. D. thesis, Dept. of Applied Mathematics, University of Washington, Seatttle, WA, (1996).

[42] D. Ueyama, *Dynamics of Self-Replicating Patterns in the One-Dimensional Gray-Scott Model*, Hokkaido Math J., **28**, No. 1, (1999), pp. 175-210.

[43] J. Wei, *On Single Interior Spike Solutions for the Gierer-Meinhardt System: Uniqueness and Stability Estimates*, Europ. J. Appl. Math., **10**, No. 4, (1999), pp. 353-378.

[44] J. Wei, *Existence, Stability and Metastability of Point Condensation Patterns Generated by the Gray-Scott System*, Nonlinearity, **12**, (1999), pp. 593-616.

[45] J. Wei, *Pattern Formations in Two-Dimensional Gray-Scott Model: Existence of Single-Spot Solutions and Their Stability*, Physica D, **148**, (2001), pp. 20-48.

[46] J. Wei, M. Winter, *Existence and Stability of Multiple Spot Solutions for the Gray-Scott Model in* $\mathbb{R}^2$, Physica D, **176**, No. 3-4, (2003), pp. 147-180.

[47] J. Wei, M. Winter, *Asymmetric Spotty Patterns for the Gray-Scott Model in* R^2, Studies in Appl. Math., **110**, No. 1, (2003), pp. 63-102.

[48] D. E. Woodward, R. C. Tyson, J. D. Murray, E. O. Budrene, H. Berg, *Spatio-Temporal Patterns Generated by Salmonella Typhimurium*, Biophysical J., **68**, (1005), pp. 2181-2189.

[49] XMORPHIA wesbite http://www.cacr.caltech.edu/ismap/image.html, R. Williams, Concurrent Supercomputing Facilities, Caltech, USA.

[50] F. M. Ytreberg, S. Mckay, *Second Mechanism for Transitions in a Reaction-Diffusion System*, Phys. Rev. E., **59**, No. 3, (1999), pp. 3376-3381.